11-2016

Influence of Land Cover Type and the Reliability of Selected Land Surface Models: A Comparison of WRF Version 3.6 Coupled to CLM Version 4.0, Noah-MP, and the Bucket Hydrology

Andrew J. Kalin
University of Nebraska - Lincoln, ajkalin7@gmail.com

INFLUENCE OF LAND COVER TYPE AND THE RELIABILITY OF SELECTED LAND SURFACE MODELS: A COMPARISON OF WRF VERSION 3.6 COUPLED TO CLM VERSION 4.0, NOAH-MP, AND THE BUCKET HYDROLOGY

By:

Andrew Kalin

A THESIS

Presented to the Faculty of

The Graduate College at the University of Nebraska

In Partial Fulfillment of Requirements

For the Degree of Master of Science

Major: Earth and Atmospheric Sciences

Under the Supervision of Professor Matthew Van Den Broeke

Lincoln, Nebraska

November 2016

INFLUENCE OF LAND COVER TYPE AND THE RELIABILITY OF SELECTED LAND SURFACE MODELS: A COMPARISON OF WRF VERSION 3.6 COUPLED TO CLM VERSION 4.0, NOAH-MP, AND THE BUCKET HYDROLOGY

Andrew Kalin, M.S.

University of Nebraska, 2016

Advisor: Matthew Van Den Broeke

In this study, the validity of 3 LSMs (Community Land Model version 4.0, Noah-MP and the Budyko Bucket Hydrology model [henceforth referred to as 'Bucket model']) coupled with the Weather Research and Forecasting model version 3.6 (WRF3.6), was examined in an effort to show the associated strengths and weaknesses of each LSM. This objective was completed by first, developing expected results based on a simple surface energy budget calculation, and by later comparing model output to Parameter-elevation Relationships on Independent Slopes Model (PRISM) data, which serve as gridded observed values of mean monthly temperature and total monthly precipitation. Model output temperature, precipitation, sensible heat (SH), latent heat (LH), downward solar radiation, and soil water content (SWC) are also compared to observations from several Atmospheric Radiation Measurement (ARM) and AmeriFlux sites across the Central and Southern Great Plains. The LSM output analysis revealed an overall warm bias in CLM4.0 and Noah-MP, with a cool bias of larger magnitude in the Bucket model. All 3 LSMs produced similar patterns of wet and dry biases when compared to each other across identical time periods, but no overall bias for any particular LSM emerged. Biases in model output of SWC, SH, LH, and downward solar radiation compared to

observations, were consistent with what would be expected based on results from the surface energy budget component of the study. While many factors should be considered when choosing a LSM, both sophisticated LSMs seem to be viable options for simulating the effects of land use change in the Southern Great Plains region, while the limitations of the Bucket model with detailed surface energy calculations make it less suitable for such a detailed study.

Acknowledgements

I would like to thank my advisor, Dr. Van Den Broeke, for all of his advice and encouragement throughout my graduate research and coursework. I would also like to thank him for his continued support of completing my graduate thesis remotely. Additionally, I am also appreciative and thankful for the support and council from my committee members, Dr. Oglesby and Dr. Rowe. This work would not have been made possible without the help of those mentioned above as well as the other members of the project, namely: Abraham Torres, Cindy Hays, and Dr. Hu. Larry McDaniel also provided invaluable knowledge on the subject of R statistical programming language. I would also like to thank my family for unwavering support of my continued education and fellow graduate and undergraduate students for providing a venue to bounce ideas off of as well as an outlet away from my research. Clint Aegerter was particularly instrumental in helping with programming and research related questions. Finally, financial support of the University of Nebraska-Lincoln Earth and Atmospheric Science Department and the National Science Foundation (Grant # AGS-1355916) as well as the computing resources provided by the National Center for Atmospheric Research's (NCAR's) Computational and Information Systems Laboratory (CISL) and the Holland Computing Center were critical in the successful completion of this research.

Table of Contents

List of Figures

Chapter 1. Introduction

I. Background

The United States' Southern Great Plains (SGP) is a region with historical precipitation extremes ranging from severe drought to flooding. These extreme events are expected to increase in frequency and magnitude with a future changing climate (Trenberth et al. 2003). Severe droughts not only affect the SGP, but cause substantial and devastating impacts all over the world (Wilhite 2000). It is therefore important to better understand the mechanisms which lead to drought occurrence and maintenance, specifically in this region. While remote forcing mechanisms are important (Schubert et al. 2004; Hu and Feng 2012), it has been shown that remote forcings alone are insufficient to maintain climate anomalies and that local-scale interactions must also be considered (e.g., Koster and Suarez 1995). To add further complexity to the local-scale interactions that must be considered, human activity such as land use/land cover (LULC) changes also play a role in the local climate and therefore in the SGP's drought susceptibility (Copeland et al. 1996; Jacobs et al. 2000).

Remote forcing mechanisms for drought can be characterized by atmospheric circulation anomalies that result from and are initiated by variations in sea surface temperature on the inter-annual to decadal time scale (Hu and Feng 2012). The El Niño-Southern Oscillation (ENSO) has been shown to strongly influence atmospheric circulations and therefore precipitation variations in the mid-latitudes of the United States with the Atlantic Multidecadal Oscillation (AMO) also playing an important role in the response to El Niño and La Niña. More specifically, North America experiences the driest conditions during La Niña in the warm phase of the AMO as flow originating from

the southwestern U.S. and Mexican Plateau suppresses summer precipitation. This continual large-scale dynamical atmospheric support is usually present during persistent drought or flood events (Mo et al.1997). In addition to its dependence on sea surface temperature variations, long-term drought in the Great Plains is also thought to be a function of deep soil memory (Oglesby et al. 2002, Schubert et al. 2004). A long term deficit in soil moisture can lead to an increase in surface temperature, therefore resulting in a reduction of surface pressure and an increase in ridging aloft.

Land-atmosphere interactions, including those influenced by land use change, have an influence on such local forcings and are a critical component of the regional climate system. Land cover changes made by humans have likely affected the near-surface climate (e.g., Copeland et al. 1996; Taylor et al. 2002). Thus, LULC changes must be considered when representing the effects of land surface properties in high-resolution, regional-scale climate models (e.g., Findell et al. 2007). Land surface processes have also been found to be critically important for severe convection forecasting in weather models (e.g., Holt et al. 2006). Of importance in these considerations are factors including but not limited to surface albedo, emissivity, leaf area index (LAI), rooting depth and canopy height (Steyaert and Knox 2008).

In particular, changes in the LAI of different vegetation affect the overall surface albedo. Land surface albedo affects the surface energy budget by influencing the amount of absorbed versus reflected solar radiation. In an energy balance equilibrium state, an increase in surface albedo will lead to a decrease in the equilibrium temperature (Pielke et al. 2001). LAI further affects the partitioning of absorbed solar radiation between latent heat (LH) and sensible heat (SH) flux from the surface (Copeland et al. 1996), known as

the Bowen ratio (Bowen 1926). The greater the LAI, the greater the influence of vegetation on the surface albedo and Bowen ratio by increasing LH relative to SH, which by altering the surface energy budget can influence regional and large-scale atmospheric circulation (e.g., Charney et al. 1975). More specifically, an increase of the local albedo would result in a decrease of absorbed energy at the surface and a response of atmospheric subsidence, therefore suppressing precipitation locally.

Soil moisture, which is influenced by land use, rooting depth, and biomass of overlying vegetation, also plays a key role in determining the Bowen ratio (e.g., Oglesby and Erickson 1989; Oglesby et al. 2001; 2002). With less soil moisture present, more energy goes into heating the ground rather than into the process of evapotranspiration (ET), or SH and LH respectively (Trenberth et al. 2003). As more energy goes into heating the dry ground, the hot surface can result in a local ridge. Air flow over this local ridge can be treated similar to air flow over a mountain barrier, with the same result of suppressed precipitation, known as the "equivalent mountain" (Stern and Malkus 1953). The presence of irrigation is another important consideration as it increases soil water content (SWC) and decreases surface temperature relative to what would occur naturally (Mahmood et al. 2006, 2008). As a result of energy partitioning differences between land cover types, mesoscale circulations may result (Pielke et al. 1991; Weaver 2004). For example, during the Bunny Fence Experiment in Australia, a difference in albedo and roughness length was observed between agricultural crops and the adjacent native vegetation, particularly during the summer months prior to harvest (Lyons et al. 1993; Nair et al. 2011). Due to these differences in surface characteristics, planetary boundary layer (PBL) height, surface energy flux, and placement of the west coast trough were

found to be a function of land cover, with convective cloud development and associated precipitation more common over native vegetation than over the agricultural region. Land surface conditions such as the relative soil moisture also play a role in the development or inhibition of deep convection and its potential precipitation effects (Chang and Wetzel 1991; Carleton et al. 2001).

It is important to note that the effect a vegetation or land use type has on the surface energy budget varies throughout the year. Since different vegetation types have different growth and senescence patterns, the temperature and moisture profiles over a particular land cover type may vary (Pielke et al. 2001; McPherson et al. 2004). Drought can have a feedback on itself by altering the characteristics of the existing land cover and therefore further altering the surface energy budget (e.g. Trenberth et al. 2003).

A key component in the study of land-atmosphere interactions may be a land surface model (LSM), which can be used to simulate the hydrological, biogeophysical, and biogeochemical processes involved in land surface-atmosphere interactions (Wei et al. 2010). Different LSMs vary in their level of complexity and the types of physical parameterizations they incorporate, and differ in the output they produce (Pitman 2003). It is therefore important to evaluate and compare LSMs before using them to study land surface-atmosphere interactions in particular regions.

When selecting a LSM, the nature of the proposed study should be a key consideration in order to ensure the strengths of the LSM align appropriately with the research objective (Luo et al. 2012). For example, in a study focused on sub-surface energy fluxes, it would be worthwhile to invest the extra computational resources needed for a more sophisticated LSM. Additionally, if performing a comprehensive

benchmarking study involving a LSM, metrics and statistical measures across several variables and scales should be used to assess model performance. To be as physically realistic as possible, LSMs have incorporated a large number of relevant physical processes. It is therefore not practical to evaluate each process individually; instead, one must identify and quantify model biases using key traceable components, such as temperature.

II. Purpose/Motivation

The purpose of this work is to analyze the relative capability of two sophisticated LSMs, Community Land Model version 4.0 (CLM4.0) and Noah-MP, along with one simple reference LSM, the Budyko Bucket Hydrology model (henceforth referred to as 'Bucket model'), to simulate temperature, precipitation and surface energy fluxes in high-resolution (4-km horizontal spatial resolution) over the Southern Great Plains (SGP) of the United States. Additionally, an analysis to determine how characteristics of different land cover types affect different terms of the surface energy budget was also performed. A better understanding of how these core terms of a basic surface energy budget are affected by different land characteristics provided a basis for expected results from the more sophisticated LSM comparison component of the study, and helped to diagnose reasons for biases observed in the model output.

There is a lack of literature on LSM comparisons for the warm season over the SGP. This study helps address this need by determining each LSM's biases and shortfalls for this region in the warm season, in an effort to improve future research. Choosing a LSM with reasonable output is particularly important for this region because the U.S. Great Plains are characterized by large precipitation variability and drought susceptibility

(Mo and Schemm 2008). The region is strongly agriculture-dependent, with agricultural activity constantly altering LULC. Examining LSM performance over the region is crucial for future studies, especially those examining the effects of LULC on changes in regional atmospheric circulations and precipitation, which could drastically influence the region's susceptibility to drought.

Chapter 2. Methods

I. Surface Energy Budget

The hypothesis that LULC change affects the surface energy/heat budget was tested by establishing a simple surface energy balance model and computing output for various land cover types. The surface energy budget equation was developed from the basic Penman-Monteith approach (Paltridge and Platt 1976) and consists of four separate terms: incoming shortwave radiation, outgoing longwave radiation, SH and LH. A fifth term representing subsurface heating was ignored to stay consistent with how more simplistic LSMs, such as the Bucket model, typically handle this subsurface heating term. In order to most easily assess the impact of altering LULC and the various biophysical characteristics that each bring, the budget was solved for temperature in the outgoing longwave radiation term. The balance can be written as:

$$H_2 = H_1 - H_3 - H_4$$

Where H_2 is the outgoing longwave radiation, H_1 is the incoming shortwave radiation, H_3 is the sensible heating and H_4 is the latent heating. Each individual term can be written as follows:

$$H_1 = (1 - n) * R * (1 - \mu)(1 - \gamma - r)$$

$$H_2 = \varepsilon\sigma T^4$$

$$H_3 = \rho C_p D * (T_s - T_a)$$

$$H_4 = \omega(\rho L_v D \left(\frac{0.622}{P}\right)(e_{sat} - e) + \alpha H_3$$

Where

n = cloud cover (zero for this study)

R = incoming solar radiation at top of the atmosphere ($1370\ \mathrm{W\ m^{-2}}$)

μ = surface albedo

γ = atmosphere absorptivity (0.17; Hanson et al. 1967)

r = atmosphere reflectivity (0.14; Hanson et al. 1967)

L_v = latent heat of vaporization ($2.5 \times 10^6\ \mathrm{J\ kg^{-1}}$)

ε = emissivity (~ 1)

σ = Stefan-Boltzmann constant ($5.67 \times 10^{-8}\ \mathrm{W\ m^{-2}\ K^{-4}}$)

T = 2-m air temperature (°C)

C_p = specific heat of air at constant pressure ($1004\ \mathrm{J\ K^{-1}\ kg^{-1}}$)

D = mixing magnitude (~ $.01\ \mathrm{ms^{-1}}$; Paltridge and Platt 1976)

T_s = surface temperature (°C)

T_a = air temperature (°C)

ω = water availability factor

e_{sat} = saturation vapor pressure (Pa)

e = vapor pressure (Pa)

ρ = density of air ($1.2\ \mathrm{kg\ m^{-3}}$)

$\left(\frac{d[esat]}{dT}\right)$ = 2.963 (for 27 °C)

And where

$$\alpha = \left(\left(\frac{L_v}{C_p}\right)\left(\frac{0.622}{P}\right)\right)\left(\frac{d[esat]}{dT}\right)$$

For this portion of the study, cloud cover was assumed to be zero and solar radiation at the top of the atmosphere was calculated for the equinox at 40° north at solar noon. The variables that were allowed to change based on land cover type were albedo, water

availability factor, vapor pressure deficit and surface-air temperature difference. The albedo and water availability factor values used were gathered from the LANDUSE.TBL used in the Weather Research and Forecasting model v. 3.6 (WRF3.6; Skamarock et al. 2008). While albedo values were held constant to those values provided in the table throughout, water availability factor was changed after an initial set of calculations were run in order to assess the impact of this variable. Varying values of vapor pressure deficit and surface-air temperature difference were also used in order to assess a warming or a cooling trend between land cover types. Because the underlying goal of this initial project component was to support a more elaborate research project on the validity of various LSMs in the Southern Great Plains, the three land type scenarios that were used were irrigated cropland, mixed irrigated/dry cropland and grassland. Irrigated and mixed cropland both have an albedo of 0.18 and a water availability factor of 0.5 and 0.25 respectively. Grassland has an albedo of 0.19 and water availability factor of 0.15.

Each term of the budget was calculated individually and then combined to ultimately solve for 2-m air temperature. Output of the value of each term and derived temperature was obtained for analysis. Various plots were also constructed to further help analyze the impact of the varying characteristics of the land cover types on the overall surface energy budget. These calculations were completed separate of the more elaborate LSM simulations to be discussed further in the next section.

II. WRF Coupled With LSMs

The most substantial component of this study used WRF3.6, coupled with three different LSMs, namely CLM4.0, Noah-MP and the Bucket model. As described in more

detail below, each LSM differs in degree of complexity and apparent capability to estimate fluxes of energy and moisture in different soil layers. In WRF3.6 a nested domain was used, with an outer domain consisting of the continental United States and surrounding waters at 12-km resolution and an inner domain that covers the U.S. central and southern Great Plains at 4-km resolution (approximately 28° - 43° N and 94° - 106° W; Fig. 2.1). Lateral boundary conditions were provided by the North American Regional Reanalysis (NARR) dataset (Mesinger et al. 2006) at a horizontal resolution of 32 km. The land use categorization in WRF3.6 was determined from the United States Geological Survey (USGS) 24 land use categories. Simulations were run for 2006, 2007, and 2012, representing a normal, wet, and dry year respectively over much of the inner domain (Table 2.1). Simulation results for the months of April, June, and August from each of these three years were chosen for analysis to examine the differences in large-scale forcing throughout the growing season.

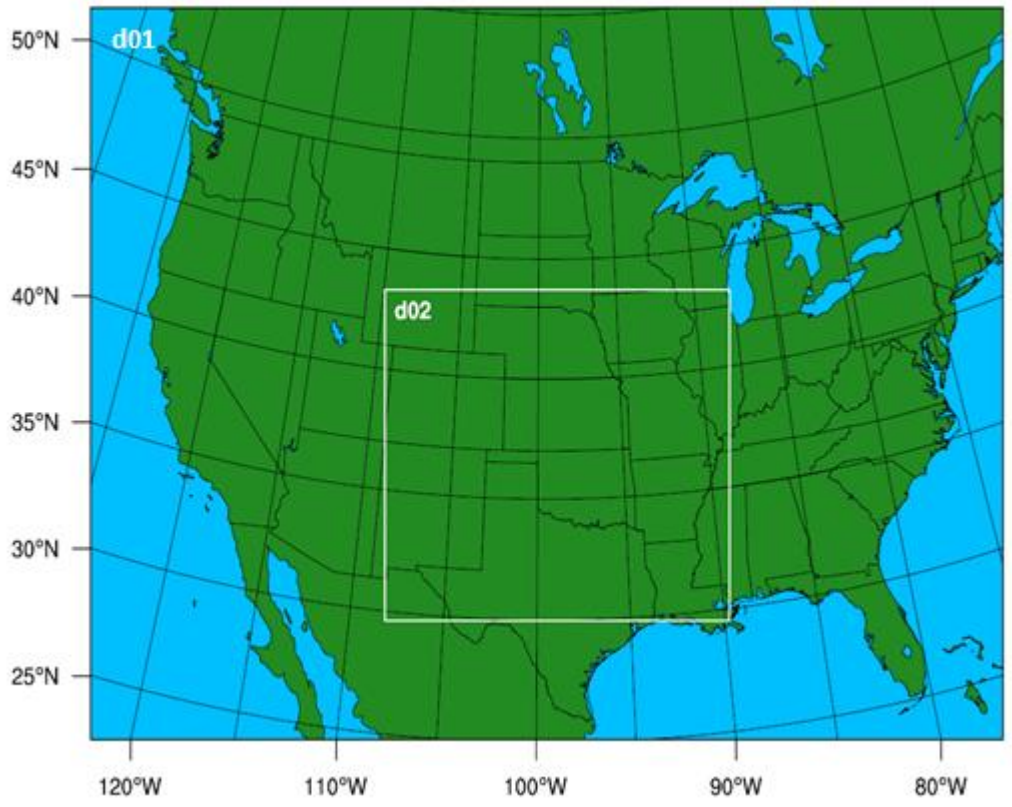

Figure 2.1: Inner (4-km; d02) and outer (12-km; d01) domain of WRF simulations.

	2 m Air Temperature (°C)				Mean Total Precipitation (mm)			
	April	**June**	**August**	**Annual**	**April**	**June**	**August**	**Annual**
2006	15.1	23.3	24.7	13.5	59.6	52.7	91.8	706.0
2007	11	22.2	25.5	12.9	69.7	99.2	79.0	827.6
2012	14.8	24.0	24.6	14.3	58.3	43.5	59.5	573.7

Table 2.1: Mean monthly and annual 2-m temperature and precipitation over the inner domain (4-km horizontal resolution) derived from PRISM data showing 2006, 2007, and 2012 to be normal, wet, and dry years respectively across the SGP.

The WRF Single-Moment 5-class scheme (Hong et al. 2004) was used for cloud microphysics, the Kain-Fritsch scheme (Kain and Fritsch 1990; Kain 2004) for cumulus parameterization, and the Dudhia (Dudhia 1989) and Rapid Radiative Transfer Model (RRTM; Mlawer et al. 1997) schemes for shortwave and longwave radiation respectively. These parameterization choices represent a combination that appears to simulate reasonably well appropriate precipitation processes and distribution across the region of interest.

CLM4.0

The Community Land Model version 4.0 was developed by the National Center for Atmospheric Research (NCAR). It consists of 5 primary sub-grid land cover types including glacier, lake, wetland, urban, and vegetation, with vegetation being subdivided into 7 primary plant functional types. Each type has a specific leaf and stem area index and canopy height (Oleson et al. 2010; Lawrence et al. 2011). CLM4.0 allows 10 vegetation types per grid cell, which can improve flux estimations over LSMs that only allow for one vegetation type per grid cell. A total of 24 land cover types are available in CLM4.0. Temperature is calculated for 15 ground layers, partitioned into 10 soil layers unevenly spaced between the top layer (0.0-0.018 m) and bottom layer (2.296-3.802 m), and 5 bedrock layers to a depth of 42 m. Soil temperature and moisture are calculated in the 10 soil layers; snow and vegetation are also simulated. Enhancements and improvements in CLM4.0 over previous versions include cooler temperature in high-organic soils, reduced albedo over forest and grassland, more robust soil moisture estimates, and greater areal snow coverage (Lawrence et al. 2011). The static vegetation

option was used for this study, which allows for seasonal changes to LAI. The dynamic vegetation model, which allows for transient changes in LULC type in response to climate was not used however, as it has not yet been fully tested.

Previous investigation (e.g., Lu and Kueppers 2012) showed that WRF v. 3 coupled with the earlier CLM v. 3.5 (WRF3-CLM3.5) generally tended to overestimate wintertime precipitation and underestimate summer precipitation when compared to observations from AmeriFlux sites. Additionally, both WRF3-CLM3.5 and WRF3 coupled to the Noah Land Surface Model (WRF3-Noah) tended to overestimate downward solar radiation, for which an underestimate of cloud cover may be responsible (Lu and Kueppers 2012). WRF3-CLM3.5 and WRF3-Noah were both shown to overestimate SH partitioning and thus produced a warm bias at the surface. When considering the western United States, WRF3-CLM3.5 did best in overall comparison to the Soil Thermal Diffusion (STD), Rapid Update Cycle (RUC), and Noah land surface schemes (Jin et al. 2010). Noah-MP, CLM3.5, and especially Noah when coupled with WRF3.5 produced a cold bias at the surface in winter in the western United States, likely due to overestimating albedo (Chen et al. 2014). All 3 LSMs overestimated precipitation compared to Snow Telemetry (SNOTEL) sites, though gauge accuracy of the SNOTEL sites may have had an influence (Chen et al. 2014). When comparing WRF3-Noah and WRF3-CLM3.5 in California, both captured the broad spatial and seasonal temperature patterns while over-predicting daily minimum temperatures, with WRF-Noah having the larger bias (Subin et al. 2011). WRF3-CLM3.5 also performed better with dew point values, but was drier than observations. Both WRF3-Noah and WRF3-CLM3.5 exhibited a high precipitation bias.

Noah-MP

Noah-MP allows multiple options to parameterize various land, atmosphere, and hydrological processes (Niu et al. 2011). It contains 4 soil layers, 3 snow layers, and 1 canopy layer, and has a sub-grid scheme to allow for gaps in the vegetation canopy. Additionally, Noah-MP features a two-stream radiation transfer scheme to allow for consideration of 3-dimensional canopy structure, and utilizes a Ball-Berry photosynthesis-based stomatal resistance. It is capable of distinguishing between C3 and C4 photosynthesis pathways. Noah-MP provides enhancements from the less advanced Noah LSM in vegetation canopy energy balance, layered snowpack, frozen soil and infiltration, soil moisture-groundwater interaction, and related runoff and vegetation phenology (Niu et al. 2011). As with CLM, the static vegetation option, which allows for seasonal changes in LAI, was imposed while the dynamic vegetation models were not used.

Bucket Model

The Bucket model (e.g., Budyko 1961; Manabe 1969) treats the land surface and underlying soil as a bucket that is filled by precipitation and snowmelt and emptied by evaporation and runoff. If the water level reaches a critical value, then the "bucket" overflows as runoff. The actual evaporation rate varies linearly between zero and the potential evaporation rate based on the water level in the bucket. The model treats an entire grid cell as homogenous, not allowing for the sub-grid features as found in CLM4.0 and Noah-MP. The more simplistic features of the Bucket model allow for easier diagnostics of results, and thus provides a good source to which other LSMs can be compared.

III. Observations

PRISM

The output produced by WRF3.6 coupled with each LSM was compared to data from the Parameter-elevation Relationships on Independent Slopes Model (PRISM), which serves as gridded observational data (Daly et al. 2008; PRISM Climate Group 2015). PRISM considers location, elevation, coastal proximity, topographic facet orientation, vertical atmospheric layer, topographic position, and orographic effectiveness of the terrain to calculate a climate-elevation regression for each digital elevation model grid cell. It provides values for monthly and annual minimum, maximum, and mean temperature and precipitation totals. The 4-km resolution PRISM data were re-gridded to a common grid for both the outer 12-km and inner 4-km domains using bilinear interpolation.

ARM and AmeriFlux Observations

Output from the inner domain of the simulations was compared to observed daily and seasonal variations in surface heat fluxes, soil water content, precipitation, and temperature at various sites from the Atmospheric Radiation Measurement (ARM) and AmeriFlux experiments. ARM is a network of highly-instrumented ground stations operated by the U.S. Department of Energy (DOE) originally developed to study cloud formation processes and their influence on radiative transfer (Huang and Liu 2015). The Lamont, Pawhuska, and Ringwood, Oklahoma, and Ashton, Kansas, sites were used for this study (Fig. 2.2). AmeriFlux is a network of sites designed to measure CO_2, water, and energy fluxes in North and South America. AmeriFlux sites at Ozark, Missouri, and

Mead, Nebraska, were used (Fig. 2.2). These sites were chosen based on their availability of a complete dataset for all 3 years of study in the primary domain.

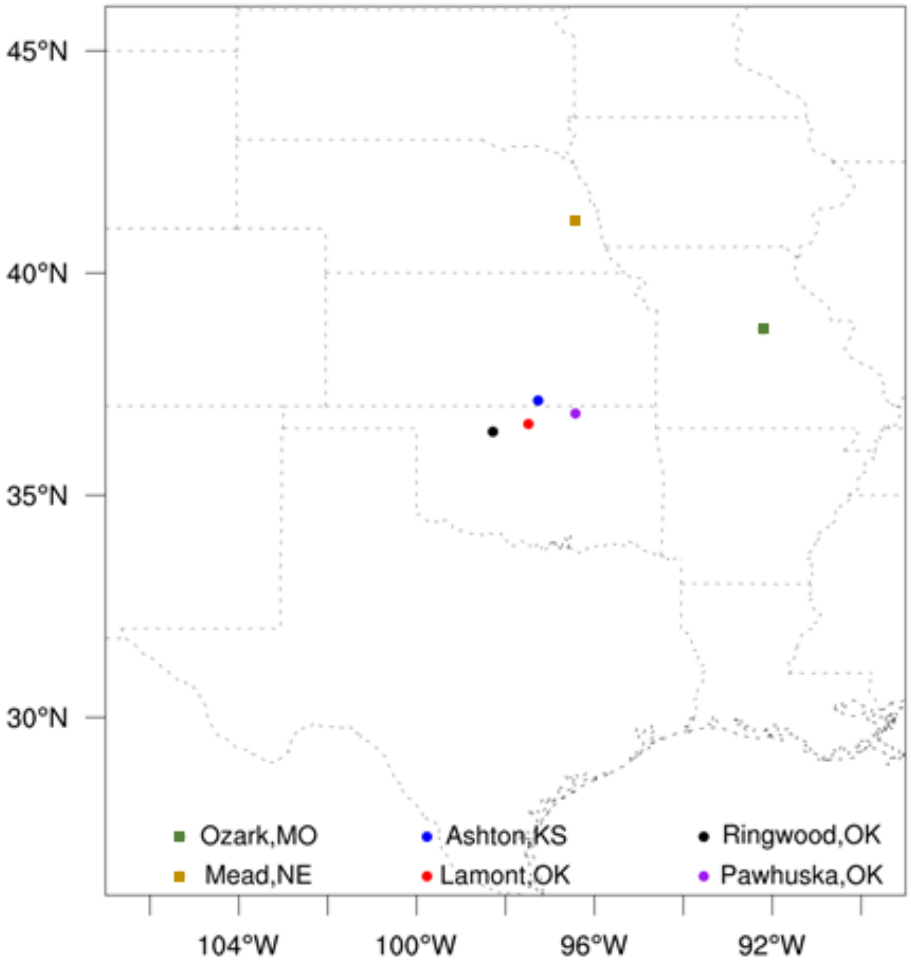

Figure 2.2: ARM (Lamont, Pawhuska, and Ringwood, in Oklahoma, and Ashton, Kansas) and AmeriFlux (Ozark, Missouri, and Mead, Nebraska) station locations.

Chapter 3. Results

I. Surface Energy Budget

An initial test of the surface energy budget's response to changes in LULC was completed in order to gain insight into what to expect in the more sophisticated LSM comparison component of the project. This examination of the surface energy budget was also used to diagnose potential reasons for various biases in the LSM output and to be sure the results were meteorologically logical. This component of the study however did not utilize any output from the LSM simulations but rather hypothetical input values for calculation within the simplistic surface energy balance model.

For these calculations, albedo and water availability were held constant to the LANDUSE.TBL (used in WRF3.6) table values, while vapor pressure deficit was allowed to vary from 0 to 10 hPa and surface-air temperature difference varied from 0 to 20 °C at a step size of 1 hPa and 1 °C respectively. The varying combinations of the two non-constant input variables produced numerous cooling or warming scenarios when transitioning from irrigated cropland to grassland. While all the output was examined, emphasis was placed on combinations that resulted in temperatures realistic for the Southern Great Plains at the equinox. A few sample warming and cooling scenarios (when transitioning from irrigated cropland to grassland) are displayed in Table 3.1 and Table 3.2 respectively.

Irrigated Cropland	Grassland
Temperature: 24.19 °C Albedo: 0.18 Water Availability Factor: 0.5 Vapor Pressure Deficit: 7 hPa Surface-Air Temperature Difference: 7 °C Incoming SW Radiation: 594.77 W/m^2 Outgoing LW Radiation: 443.19 W/m^2 Sensible Heating: 84.34 J/kg Latent Heating: 67.25 J/kg	Temperature: 25.84 °C Albedo: 0.19 Water Availability Factor: 0.15 Vapor Pressure Deficit: 9 hPa Surface-Air Temperature Difference: 9 °C Incoming SW Radiation: 587.52 W/m^2 Outgoing LW Radiation: 453.15 W/m^2 Sensible Heating: 108.43 J/kg Latent Heating: 25.94 J/kg
Temperature: 29.99 °C Albedo: 0.18 Water Availability Factor: 0.5 Vapor Pressure Deficit: 5 hPa Surface-Air Temperature Difference: 6 °C Incoming SW Radiation: 594.76 W/m^2 Outgoing LW Radiation: 478.84 W/m^2 Sensible Heating: 72.28 J/kg Latent Heating: 43.64 J/kg	Temperature: 31.23 °C Albedo: 0.19 Water Availability Factor: 0.15 Vapor Pressure Deficit: 10 hPa Surface-Air Temperature Difference: 6 °C Incoming SW Radiation: 587.52 W/m^2 Outgoing LW Radiation: 486.74 W/m^2 Sensible Heating: 72.29 J/kg Latent Heating: 28.48 J/kg
Temperature: 21.52 °C Albedo: 0.18 Water Availability Factor: 0.5 Vapor Pressure Deficit: 10 hPa Surface-Air Temperature Difference: 6 °C Incoming SW Radiation: 594.77 W/m^2 Outgoing LW Radiation: 427.52 W/m^2 Sensible Heating: 72.29 J/kg Latent Heating: 94.96 J/kg	Temperature: 24.06 °C Albedo: 0.19 Water Availability Factor: 0.15 Vapor Pressure Deficit: 9 hPa Surface-Air Temperature Difference: 10 °C Incoming SW Radiation: 587.52 W/m^2 Outgoing LW Radiation: 442.42 W/m^2 Sensible Heating: 120.48 J/kg Latent Heating: 24.62 J/kg
Temperature: 12.63 °C Albedo: 0.18 Water Availability Factor: 0.5 Vapor Pressure Deficit: 10 hPa Surface-Air Temperature Difference: 10 °C Incoming SW Radiation: 594.77 W/m^2 Outgoing LW Radiation: 378.22 W/m^2 Sensible Heating: 120.48 J/kg Latent Heating: 96.06 J/kg	Temperature: 17.08 °C Albedo: 0.19 Water Availability Factor: 0.15 Vapor Pressure Deficit: 6 hPa Surface-Air Temperature Difference: 14 °C Incoming SW Radiation: 587.52 W/m^2 Outgoing LW Radiation: 402.29 W/m^2 Sensible Heating: 168.67 J/kg Latent Heating: 16.56 J/kg

Table 3.1: Sample input conditions and output results that were typical of the set of scenarios that led to warming going from Irrigated Cropland to Grassland land use type.

Irrigated Cropland	Grassland
Temperature: 21.23 °C Albedo: 0.18 Water Availability Factor: 0.5 Vapor Pressure Deficit: 9 hPa Surface-Air Temperature Difference: 9 °C Incoming SW Radiation: 594.77 W/m^2 Outgoing LW Radiation: 425.82 W/m^2 Sensible Heating: 108.43 J/kg Latent Heating: 60.52 J/kg	Temperature: 20.18 °C Albedo: 0.19 Water Availability Factor: 0.15 Vapor Pressure Deficit: 2 hPa Surface-Air Temperature Difference: 13 °C Incoming SW Radiation: 587.52 W/m^2 Outgoing LW Radiation: 419.77 W/m^2 Sensible Heating: 156.62 J/kg Latent Heating: 11.13 J/kg
Temperature: 26.23 °C Albedo: 0.18 Water Availability Factor: 0.5 Vapor Pressure Deficit: 7 hPa Surface-Air Temperature Difference: 6 °C Incoming SW Radiation: 594.76 W/m^2 Outgoing LW Radiation: 455.51 W/m^2 Sensible Heating: 77.28 J/kg Latent Heating: 66.97 J/kg	Temperature: 25.92 °C Albedo: 0.19 Water Availability Factor: 0.15 Vapor Pressure Deficit: 5 hPa Surface-Air Temperature Difference: 10 °C Incoming SW Radiation: 587.52 W/m^2 Outgoing LW Radiation: 453.61 W/m^2 Sensible Heating: 120.48 J/kg Latent Heating: 13.42 J/kg
Temperature: 40.22 °C Albedo: 0.18 Water Availability Factor: 0.5 Vapor Pressure Deficit: 3 hPa Surface-Air Temperature Difference: 2 °C Incoming SW Radiation: 594.77 W/m^2 Outgoing LW Radiation: 546.80 W/m^2 Sensible Heating: 24.09 J/kg Latent Heating: 23.88 J/kg	Temperature: 39.77 °C Albedo: 0.19 Water Availability Factor: 0.15 Vapor Pressure Deficit: 7 hPa Surface-Air Temperature Difference: 2 °C Incoming SW Radiation: 587.52 W/m^2 Outgoing LW Radiation: 543.66 W/m^2 Sensible Heating: 24.09 J/kg Latent Heating: 19.76 J/kg
Temperature: 16.76 °C Albedo: 0.18 Water Availability Factor: 0.5 Vapor Pressure Deficit: 4 hPa Surface-Air Temperature Difference: 14 °C Incoming SW Radiation: 594.77 W/m^2 Outgoing LW Radiation: 400.53 W/m^2 Sensible Heating: 168.67 J/kg Latent Heating: 25.57 J/kg	Temperature: 9.82 °C Albedo: 0.19 Water Availability Factor: 0.15 Vapor Pressure Deficit: 2 hPa Surface-Air Temperature Difference: 18 °C Incoming SW Radiation: 587.52 W/m^2 Outgoing LW Radiation: 363.56 W/m^2 Sensible Heating: 216.86 J/kg Latent Heating: 7.09 J/kg

Table 3.2: Sample input conditions and output results that were typical of the set of scenarios that led to cooling going from Irrigated Cropland to Grassland land use type.

As would be expected, the higher water availability factor of the irrigated cropland led to a higher partitioning to LH versus that of grassland. This higher partitioning to LH negatively affected the outgoing LW radiation term, holding all other factors equal. It is also worth noting that, while expected, a higher albedo led to a lower magnitude of incoming SW radiation absorbed and thus less energy to partition between the other terms. This ultimately led to a cooler 2-m air temperature, again, holding all other factors equal. Additionally, for both the warming and cooling scenarios, irrigated cropland tended to have a higher vapor pressure deficit (VPD) and lower surface-air temperature differences compared to grassland. This would seemingly indicate the presence of dry ambient air with ongoing active ET from vegetation and moist soil. There also appeared to be a general shift toward lower surface-air temperature differences for warming scenarios. This result seems logical as a lower surface-air temperature difference, and a consistent or potentially even slight decrease in VPD, would lead to both a small SH and LH term, resulting in more outgoing LW radiation (i.e. warming). With albedo being held constantly lower for irrigated cropland and thus more incoming shortwave radiation absorbed, the magnitude of the change in VPD and surface-air temperature differences determined the warming or cooling outcome, further limiting the robustness of the results.

While this component of the study only revealed very simplistic and overall expected results, its intentions were rather to provide a basis on which to compare the more sophisticated LSM output to. By having a solid understanding of how core terms of the surface energy budget affect each other, potential reasons for biases in the LSM output were able to be later diagnosed.

II. WRF Coupled with LSMs

The broader motivation for this study was to evaluate the large-scale strengths and weaknesses of each LSM coupled with WRF3.6. To accomplish this, mean monthly temperature and total monthly precipitation values from each WRF3.6/LSM combination were compared directly to PRISM data and indirectly to NARR data for the inner domains. Since boundary conditions for the WRF simulations were provided by NARR data, it was important that this reanalysis data matched closely with the PRISM data to which the model output was being directly compared. While a plethora of variables are used, computed, and output by the LSM and regional atmospheric models, temperature and precipitation have the broadest and most complete observation records and thus provide the best tracers of model performance.

2-m Temperature

For the 3 simulated years, CLM4.0 and Noah-MP generally showed a warm bias compared directly to PRISM data and indirectly to NARR data (Fig. 3.1-3.3, 3.5-3.10, Table 3.3). These results are similar in both sign and magnitude to those obtained by Lu and Kueppers (2012) using WRF3-CLM3.5. Conversely, when coupled to WRF3.6, the Bucket model showed a cool bias, usually of larger magnitude than that of the warm bias in CLM4.0 and Noah-MP. It is also important to note that the spatial 2-m temperature and bias patterns between CLM4.0 and Noah-MP were similar, while the Bucket model produced different spatial patterns (Fig. 3.1-3.3, 3.5-3.10). These results suggest that processes responsible for these biases are similar between CLM4.0 and Noah-MP, but differ from those of the Bucket model.

The magnitude of each LSM's temperature bias increased as the summer progressed in all 3 simulated years. Each LSM generally performed best in April, and worst in the summer months of either June or August (Fig. 3.1-3.3-3.5-3.10, Table 3.3). Similarly, the cool bias in the Bucket model was consistently largest in the north central United States in April, and spread south as the summer growing season progressed. The other two more sophisticated LSMs, CLM4.0 and Noah-MP, did not have a similar spatial and temporal pattern. These early season differences could be a function of how each respective model handles snow melt, and more importantly, ground temperatures and thawing at different levels. Since CLM4.0 and Noah-MP have better capabilities when it comes to the number of soil layers they utilized, one would expect them to perform better compared to the Bucket model during the April simulations, although this did not always appear to be the case. Additionally, the relative minimum bias in all 3 LSMs compared to the rest of the year could be attributable to the weak land surface energy and moisture exchanges during this portion of the growing season. Actively growing vegetation is limited during the month of April compared to the other two simulated months. Therefore, the way each LSM handles vegetation and its resultant impacts on the atmosphere, which is a key difference between the Bucket model and the two sophisticated models, would not be as important of a factor on the model output.

It is also worth noting that in April of all 3 years, while coarser resolution, the NARR data appeared to be slightly warmer than the PRISM data (Fig. 3.1-3.3; e.g. the northward placement of the 14-16 °C isotherm). Since NARR data provided the initial boundary conditions for the WRF simulations, the slightly warmer temperatures in the NARR data compared to PRISM could have manifest themselves in the LSM output,

perhaps adding to the warm bias in CLM4.0 and Noah-MP. NARR and PRISM data appeared to match in spatial pattern fairly well in June and August of the 3 simulation years (Fig. 3.5-3.10).

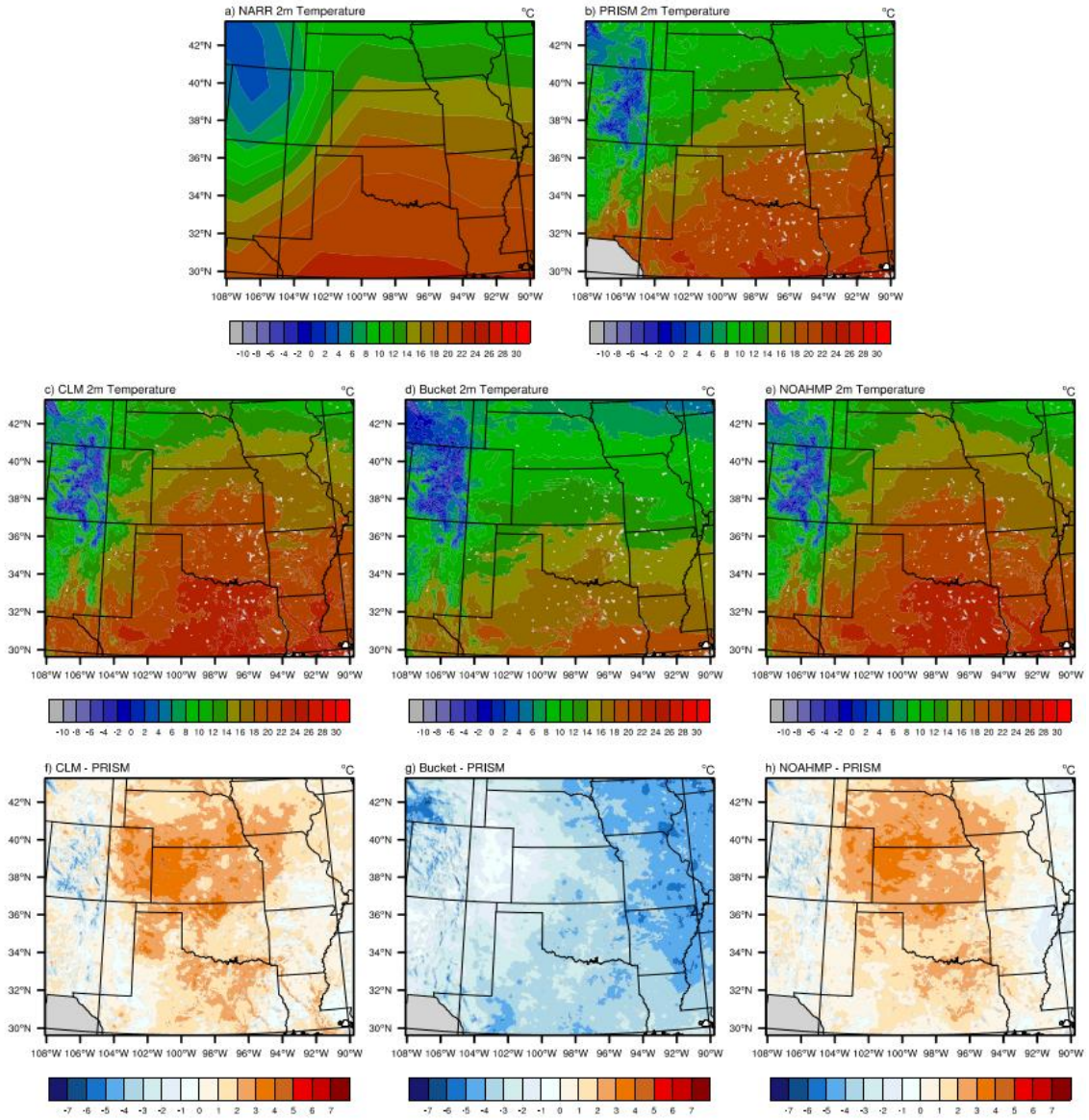

Figure 3.1: Spatial temperature distribution (°C) for April 2006. (a) NARR, (b) PRISM, (c-e) model output from CLM4.0, Bucket, and Noah-MP, and (f-h) model bias (model minus PRISM). The white areas located throughout the plots coincide with bodies of water.

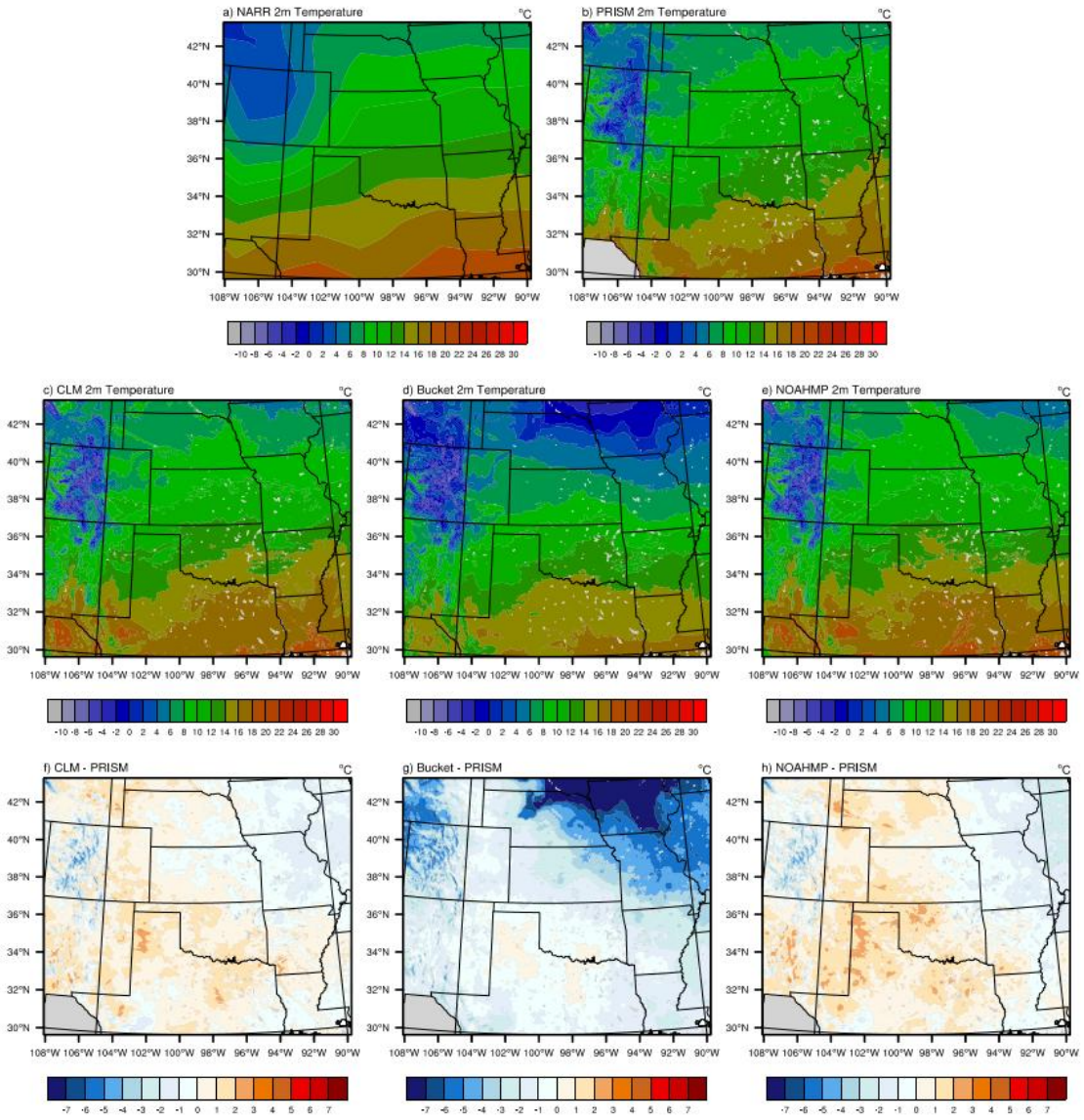

Figure 3.2: As in Fig. 3.1, except spatial temperature distribution (°C) for April 2007.

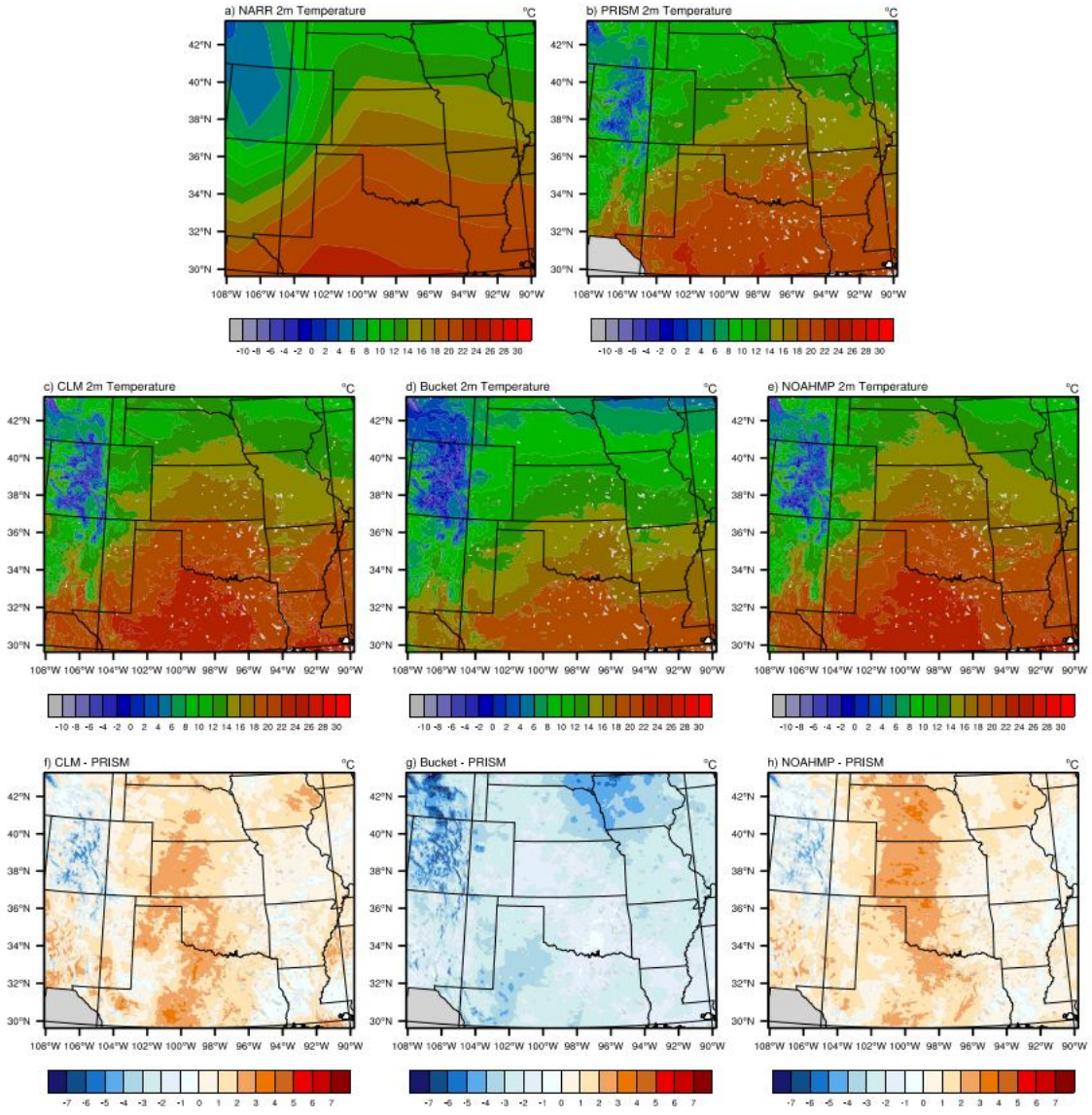

Figure 3.3: As in Fig. 3.1, except spatial temperature distribution (°C) for April 2012.

Also similar in all 3 years of simulations of the Bucket model, was the presence of a negative temperature bias in June from north central Texas through central and eastern Oklahoma into southeastern Kansas (Fig. 3.5-3.7). This area aligns closely with the savanna land cover type, perhaps indicating that during this time period, the Bucket model better represented the SWC of a generic land surface type dominated by a

combination of grasses and trees (Fig. 3.4). Key land surface characteristics, such as albedo, SWC, and emissivity, were compared to the land cover types surrounding this region of savanna and examined in terms of the surface energy budget discussed in section I. However, no significant differences or conclusive results were discovered and thus a clear explanation for this result is not apparent.

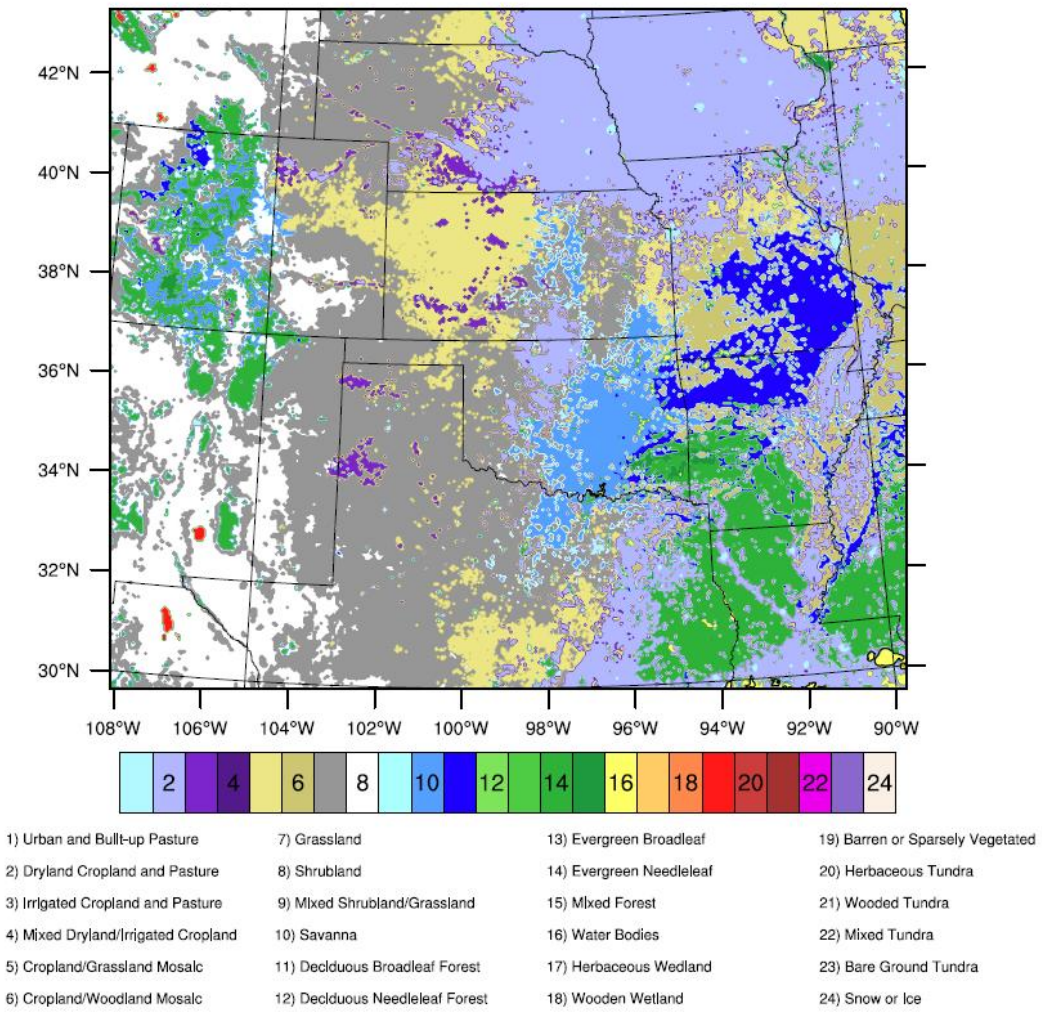

Figure 3.4: Land use (USGS 24 land use categories) in WRF3.6. Savanna land cover classification (10) is a light blue color primarily over eastern Oklahoma and adjacent areas.

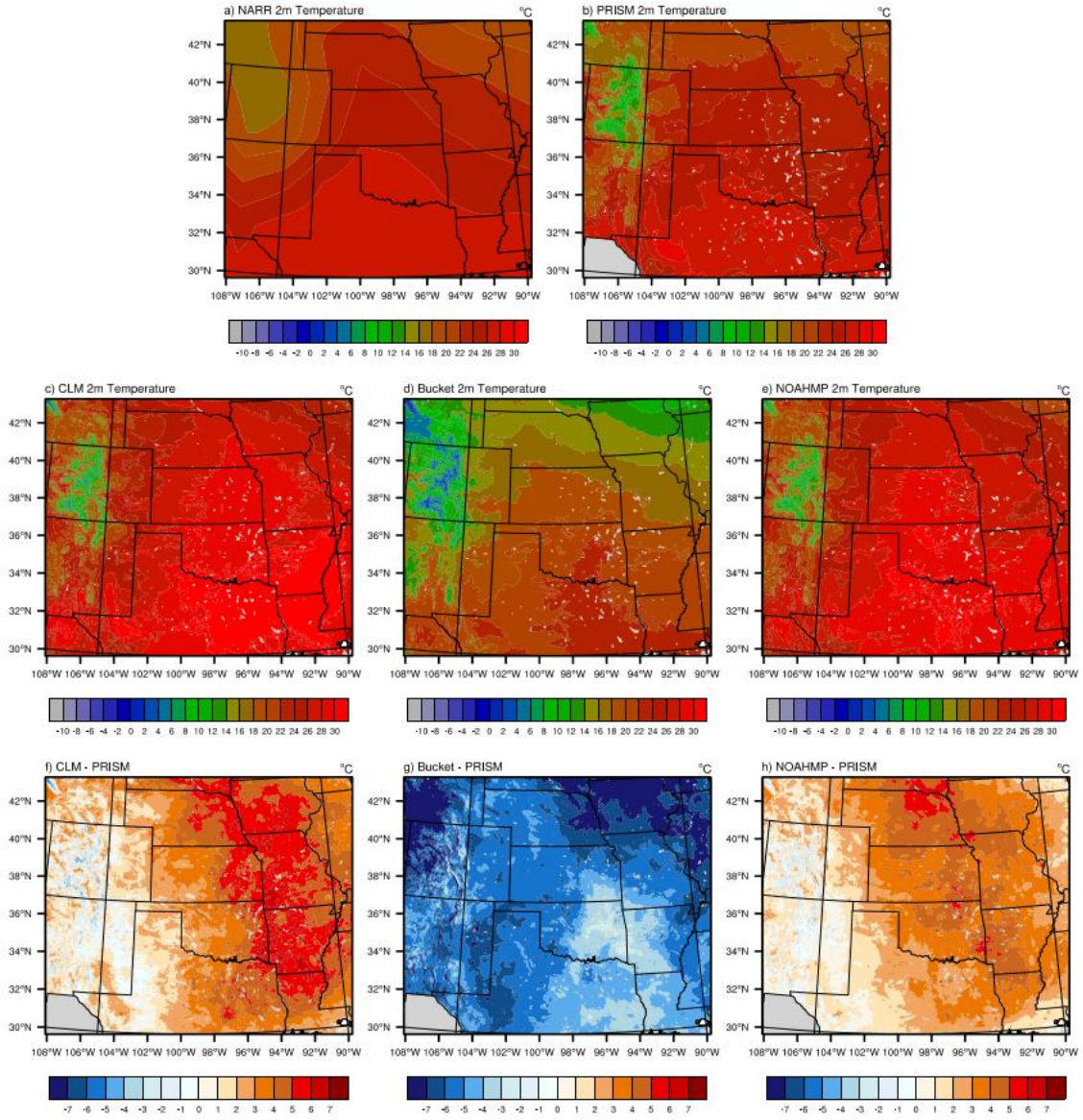

Figure 3.5: As in Fig. 3.1, except spatial temperature distribution (°C) for June 2006.

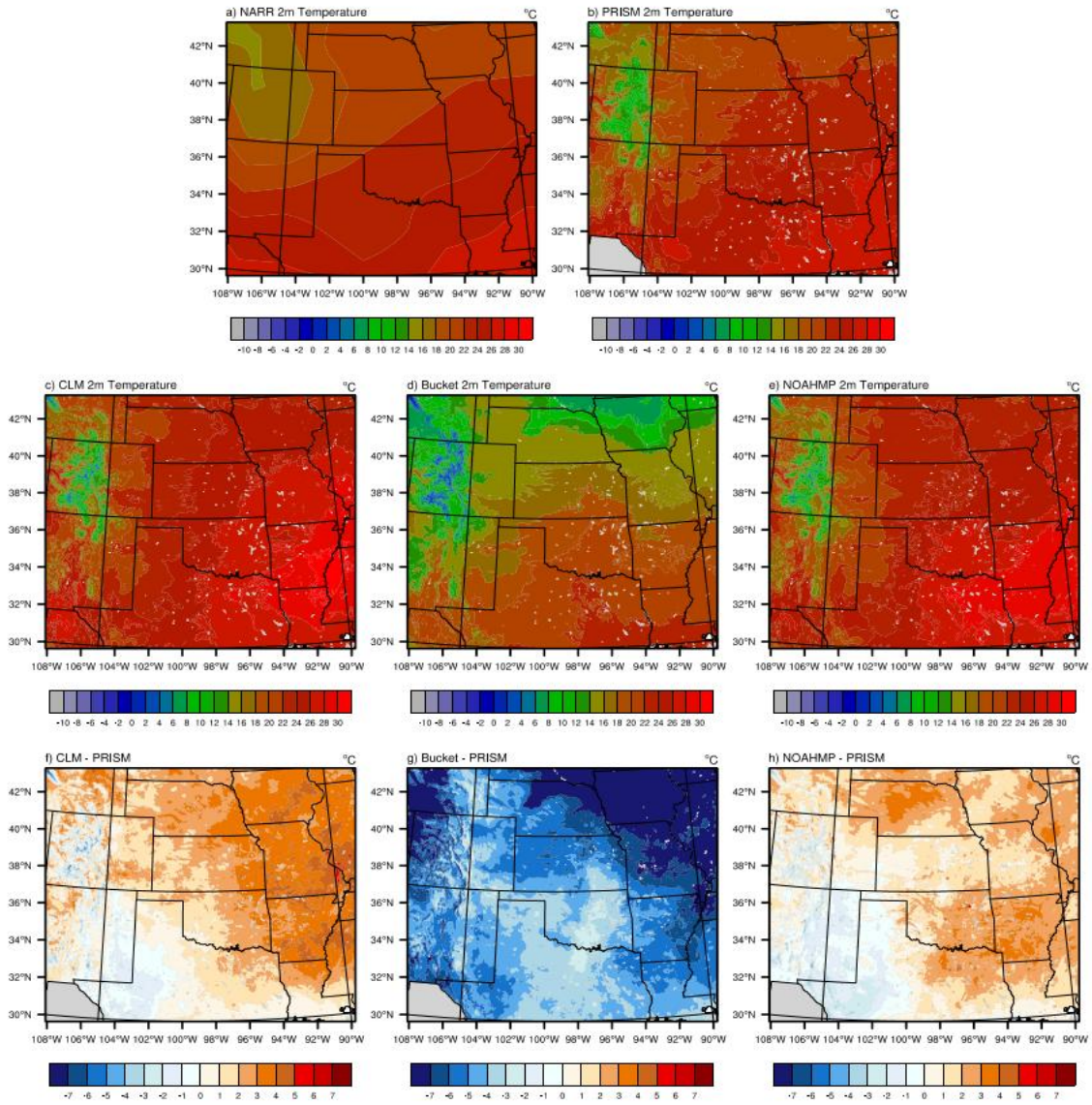

Figure 3.6: As in Fig. 3.1, except spatial temperature distribution (°C) for June 2007.

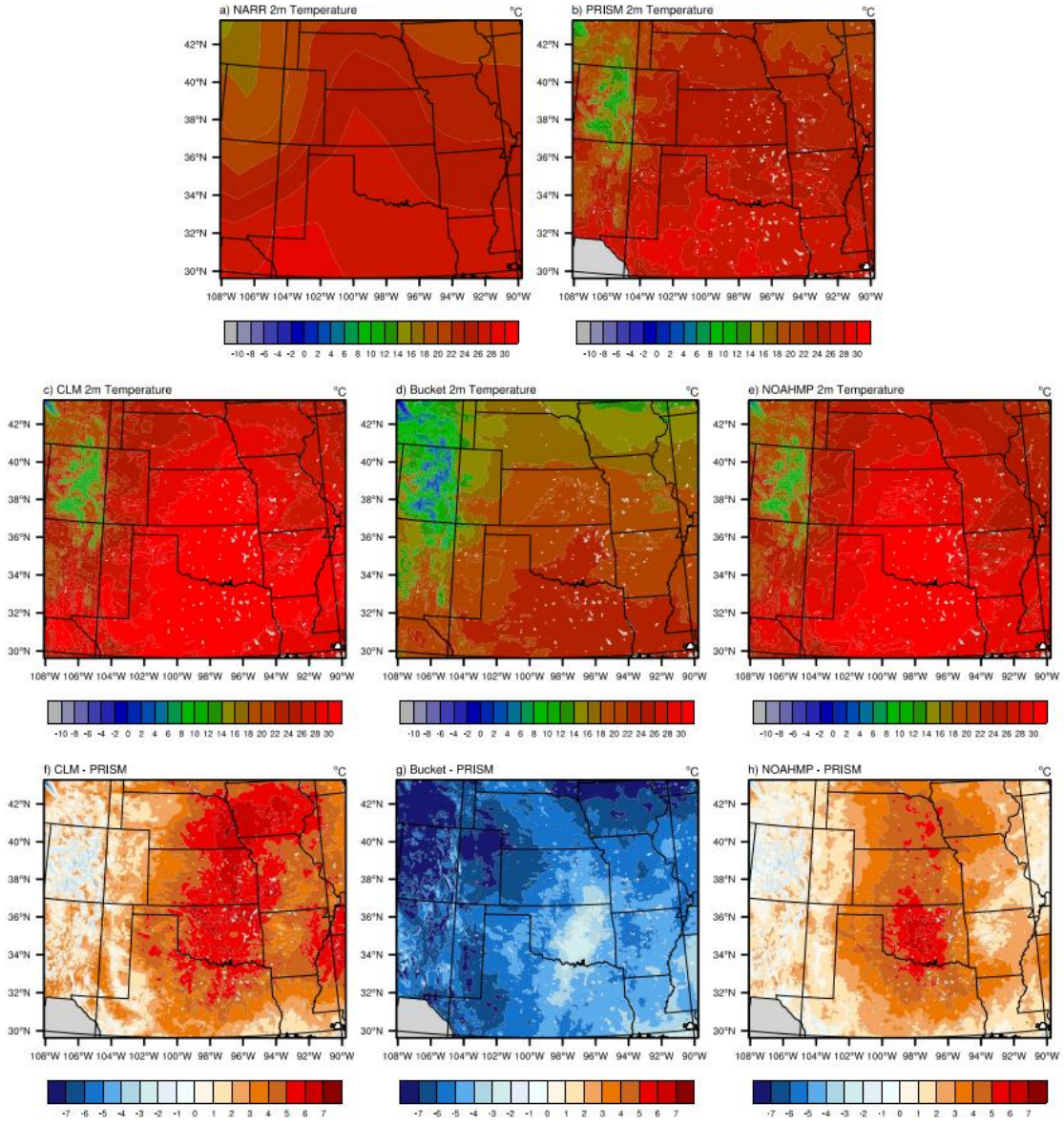

Figure 3.7: As in Fig. 3.1, except spatial temperature distribution (°C) for June 2012.

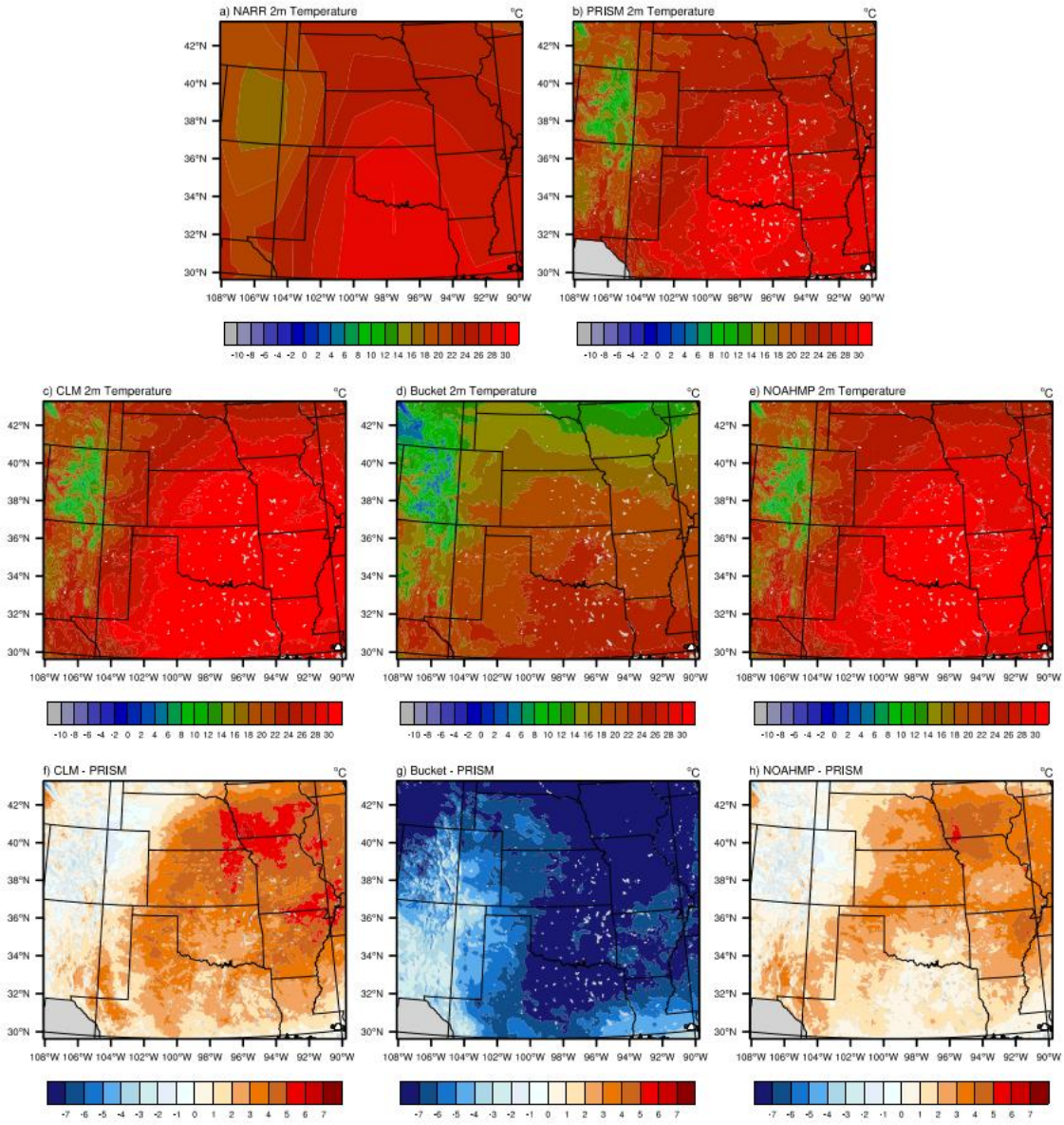

Figure 3.8: As in Fig. 3.1, except spatial temperature distribution (°C) for August 2006.

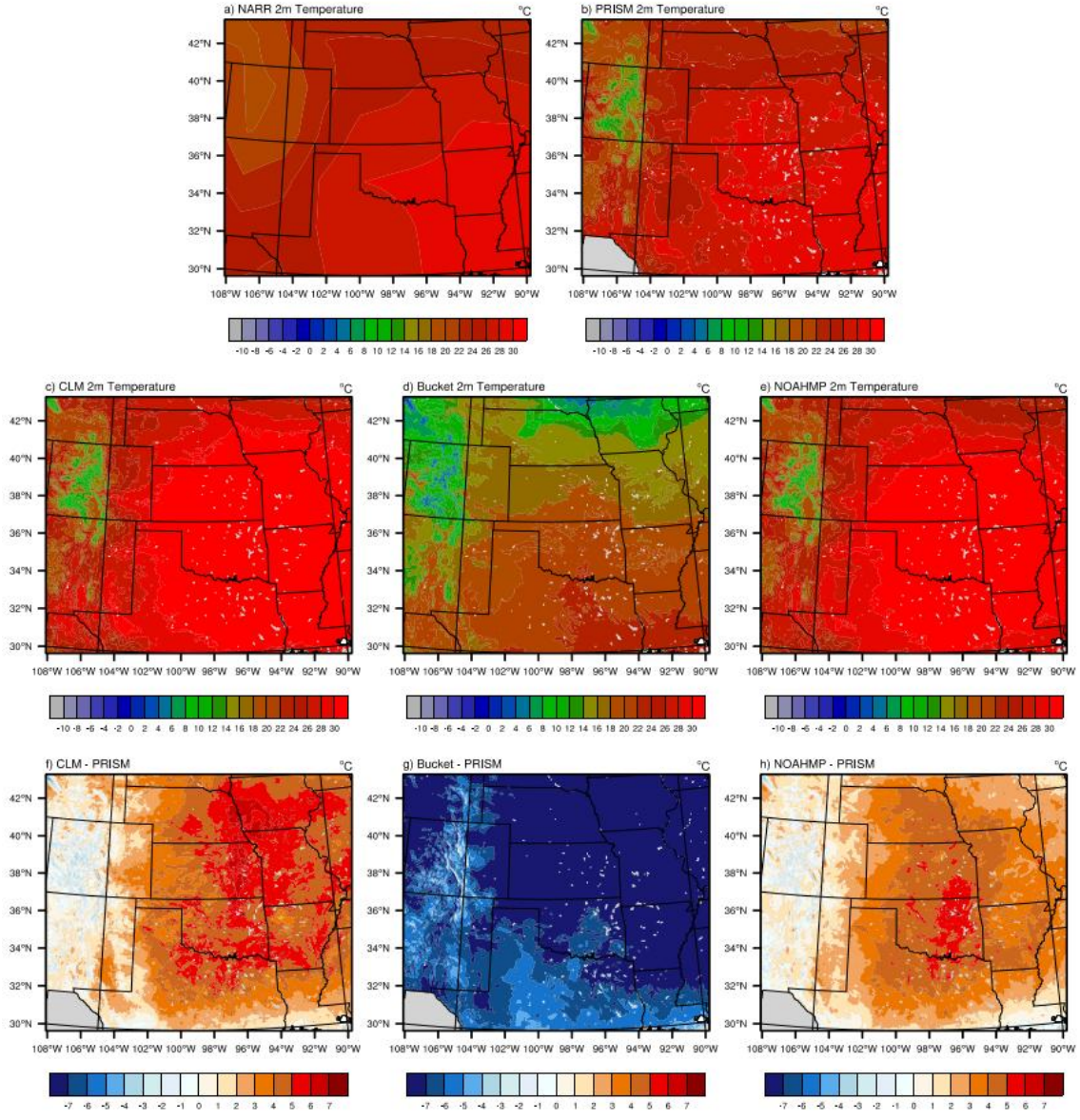

Figure 3.9: As in Fig. 3.1, except spatial temperature distribution (°C) for August 2007.

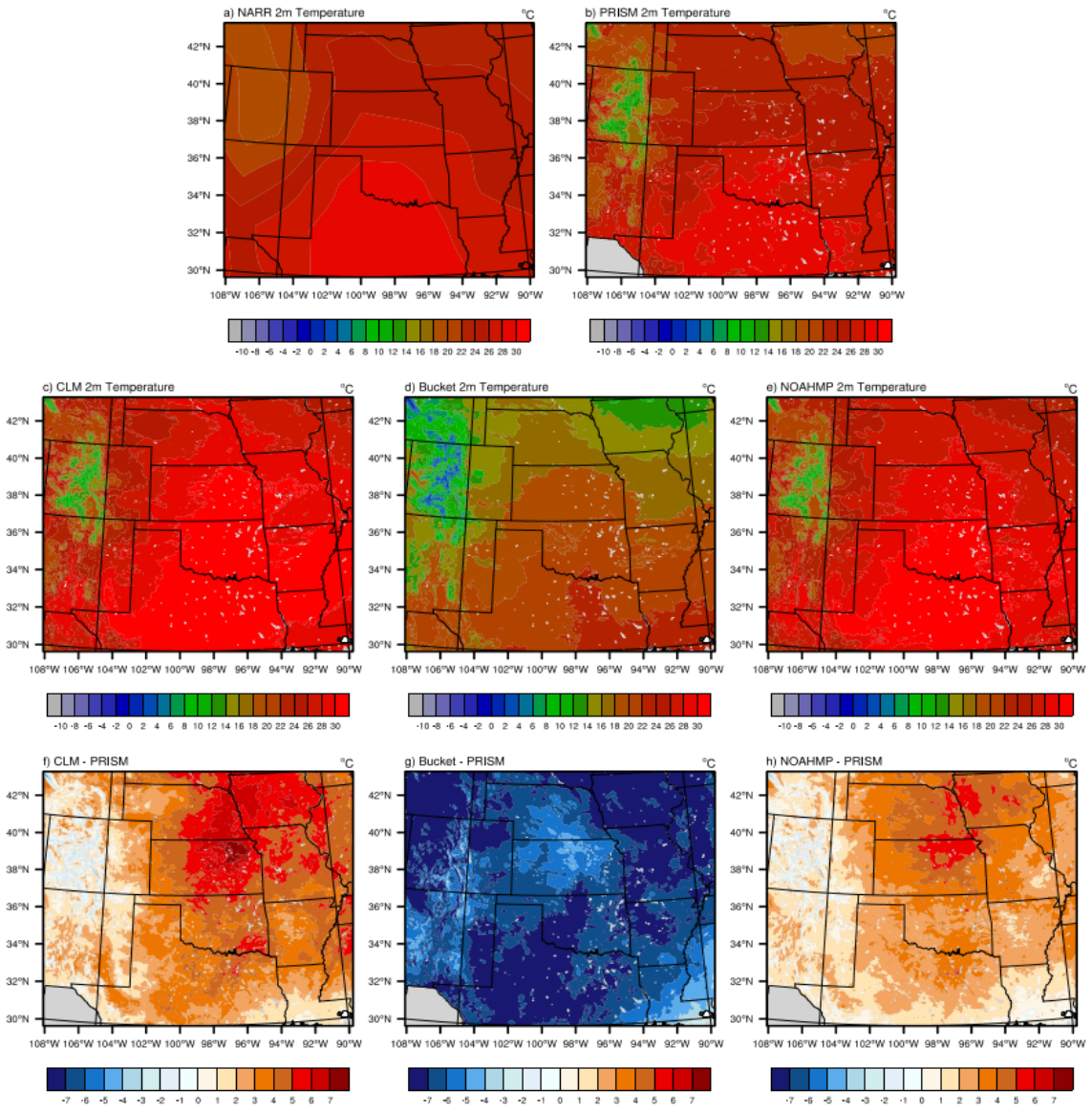

Figure 3.10: As in Fig. 3.1, except spatial temperature distribution (°C) for August 2012.

Precipitation

Each LSM's precipitation output, along with their associated biases, could be characterized as having a large degree of variation in their spatial and temporal patterns. This is to be expected when averaging precipitation over an entire month, in a region that is prone to convection. How each LSM handles variables such as soil moisture and ET

will affect the near surface parameters, as was confirmed in the surface energy budget component of this project. These resultant surface parameters will in turn affect whether or not the cumulus scheme is triggered and precipitation results. Additionally, observed precipitation from convection is usually localized in nature and thus results in monthly precipitation plots with high-precipitation regions contrasted with low-precipitation regions immediately adjacent.

With the previously mentioned caveats in mind, each LSM produced generally similar precipitation patterns, along with associated wet and dry biases over the SGP when compared to PRISM and indirectly to NARR data (Fig. 3.11-3.13). Similar to temperature, the largest differences in precipitation were between CLM4.0/Noah-MP and the Bucket model. Both CLM4.0 and Noah-MP are more complex in how they calculate soil moisture, allowing for multiple soil layers to be used and ground water fluxes to be considered. This is in contrast to the Bucket model which has an evaporation rate restricted based on the proportion of soil water content to the "field capacity" and thus the potential for overestimation of soil moisture, particularly in dry years. As was confirmed in section I, higher soil moisture will lead to a higher partitioning to LH and will artificially increase ET in the model. This enhancement in environmental water vapor could cause the model to produce precipitation during otherwise dry conditions. Another way soil moisture and ET could be enhanced over observed values is with each LSMs handling, or lack thereof, of human activities such as irrigation. This idea of overestimation of soil moisture and ET will be further discussed when examining observed surface energy fluxes.

Unlike temperature data for April in the 3 simulation years, NARR and PRISM data closely coincide spatially, keeping in mind the coarser resolution of NARR data (Fig 3.11-3.13). This is important as a wet or dry bias in NARR, the data used for providing initial conditions for the WRF simulations, could have an impact on resulting soil moisture produced by the 3 LSMs coupled to WRF. The impact of soil moisture on various surface energy fluxes is discussed further in the next section. With this in mind, however, use of NARR data did not appear to be a contributing factor in any precipitation related biases.

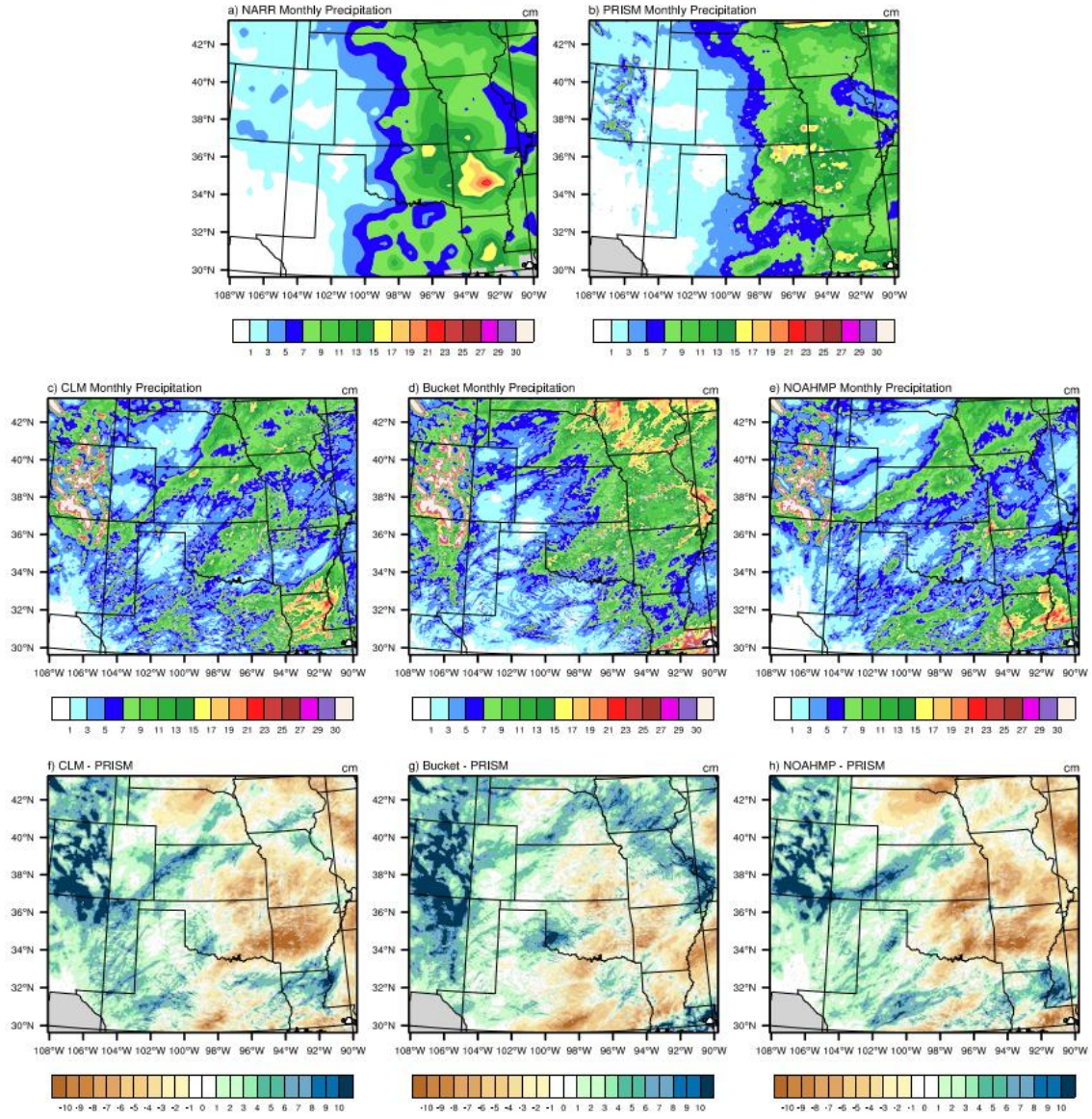

Figure 3.11: Spatial precipitation distribution in cm for April 2006. (a) NARR, (b) PRISM, (c-e) model output from CLM4.0, Bucket, and Noah-MP, and (f-h) model bias (model minus PRISM).

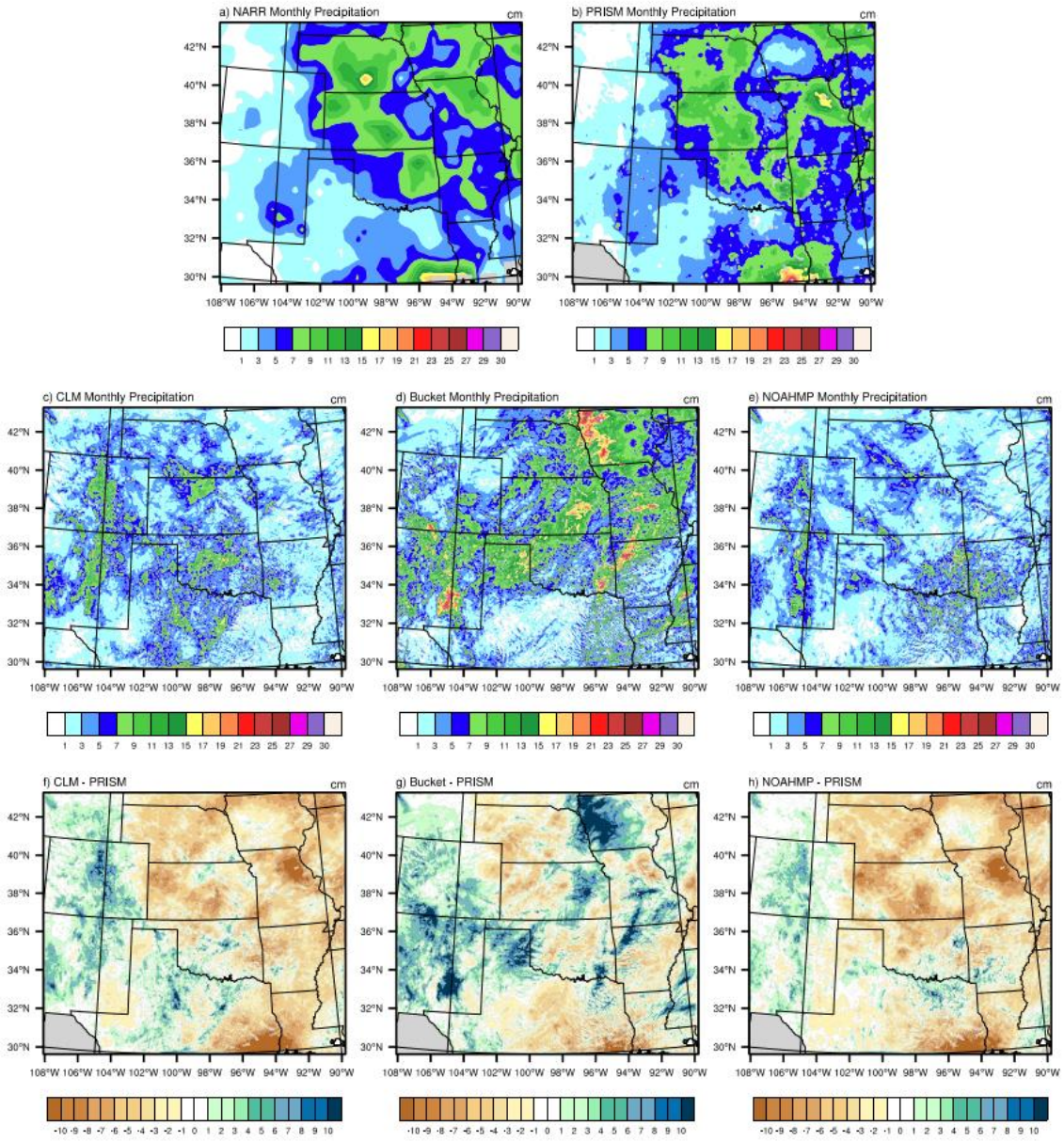

Figure 3.12: As in Fig. 3.11, except spatial precipitation distribution (cm) for June 2006.

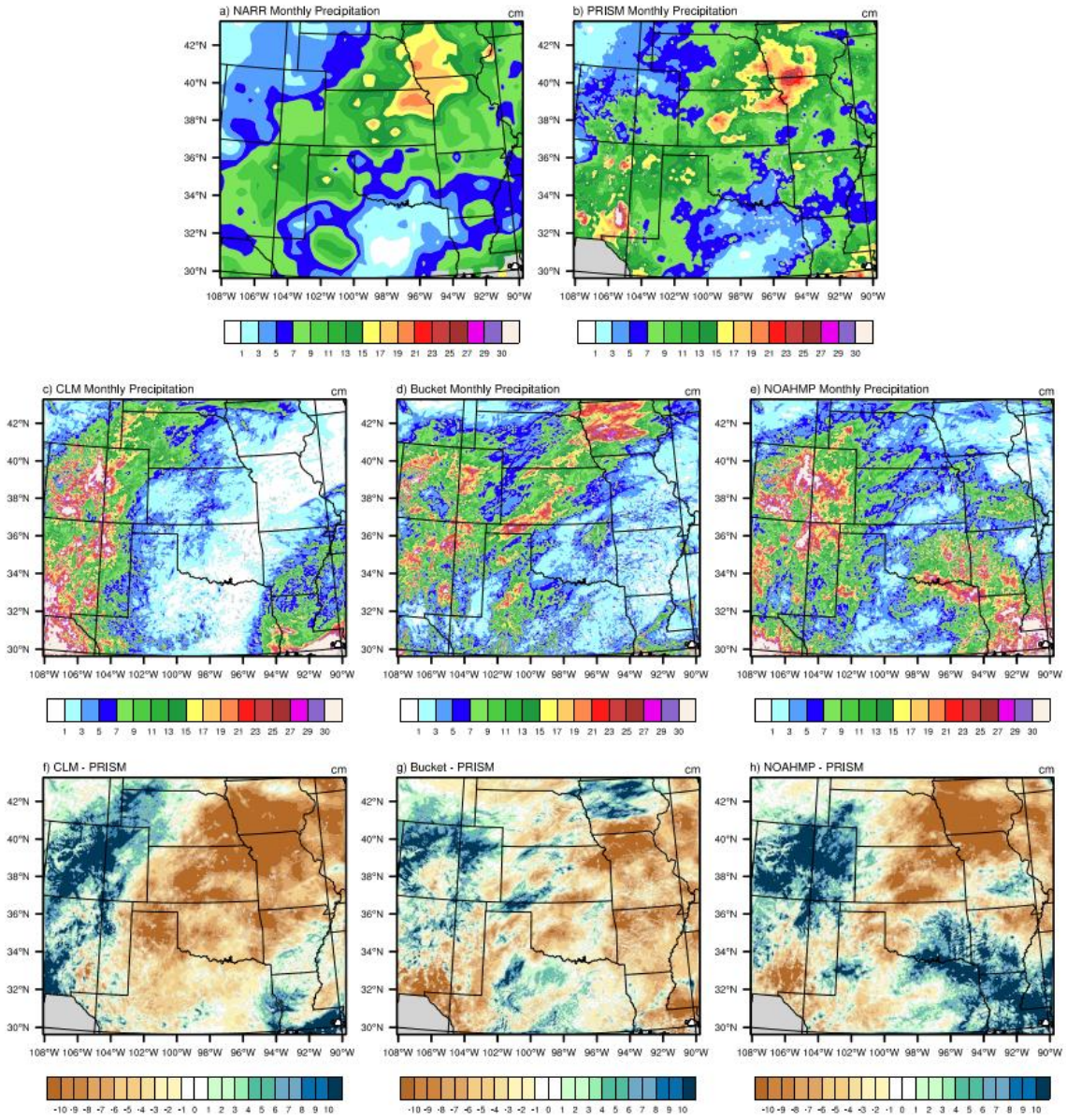

Figure 3.13: As in Fig. 3.11, except spatial precipitation distribution (cm) for August 2006.

Quantitative Comparison across the Inner Domain and to Point Observational Data

In order to quantitatively compare the WRF3.6-LSM results to PRISM data, the mean 2-m air temperature and monthly total precipitation for the inner 4-km domain were calculated from the WRF3.6-CLM4.0, -Noah-MP, and -Bucket model simulations. These

domain-averaged values were compared to PRISM data averaged over the inner domain, with associated bias and standard deviation values also being computed. As anticipated, the comparison yielded results that were consistent with those described above for temperature and precipitation (Fig. 3.1-3.3, 3.5-3.10). For April of the three simulated years, CLM4.0/Noah-MP were about 1 °C warmer and the Bucket model 2-3 °C cooler than PRISM (Table 3.3). In June and August, CLM4.0/Noah-MP averaged 2-3 °C warmer than PRISM, while the Bucket model was 5-8 °C cooler than PRISM. These temperature biases were typically within one standard deviation of each data set and thus which model performed best in each month of each year was not able to be definitively determined. However, the consistent warm bias in CLM4.0/Noah-MP and cool bias in Bucket, with increasing magnitude through the growing season, is still evident.

2 m Air Temperature (°C)

	2006								
	April			June			August		
	Mean	Bias	SD	Mean	Bias	SD	Mean	Bias	SD
PRISM	15.1	--	4.9	23.3	--	3.4	24.7	--	4.2
CLM4.0	16.4	+1.3	5.3	26.4	+3.1	4.3	27.1	+2.4	5.2
Noah-MP	16.2	+1.1	5.3	25.9	+2.6	4.0	26.5	+1.8	4.8
Bucket	12.0	-3.1	4.8	17.7	-5.6	4.1	18.1	-6.6	4.2
	2007								
	April			June			August		
	Mean	Bias	SD	Mean	Bias	SD	Mean	Bias	SD
PRISM	11	--	4.1	22.2	--	3.5	25.5	--	3.5
CLM4.0	11.3	+0.3	4.4	24.1	+1.9	4.0	28.8	+3.3	4.9
Noah-MP	11.4	+0.4	4.5	23.4	+1.2	4.0	28.2	+2.7	4.7
Bucket	8.6	-2.4	5.4	16.5	-5.7	4.5	17.2	-8.3	4.3
	2012								
	April			June			August		
	Mean	Bias	SD	Mean	Bias	SD	Mean	Bias	SD
PRISM	14.8	--	4.6	24.0	--	3.3	24.6	--	3.5
CLM4.0	15.8	+1.0	5.2	27.6	+3.6	4.3	27.9	+3.3	4.2
Noah-MP	15.8	+1.0	5.1	26.6	+2.6	4.2	27.1	+2.5	3.8
Bucket	12.3	-2.5	5.2	18.4	-5.6	4.2	17.7	-6.9	3.9

Table 3.3: Mean monthly 2-m temperature, bias compared to PRISM, and standard deviation over the inner domain (4-km horizontal resolution) for the months of April, June, and August of 2006, 2007, and 2012.

No clear pattern in precipitation biases are seen between CLM4.0, Noah-MP and the Bucket model (Table 3.4). Again, the associated biases are generally within one standard deviation of the data set as a whole and, thus, definitive conclusions as to the models' performance cannot be made. The largest difference between the two sophisticated LSMs and the Bucket model occurred during 2012, a dry year. As noted prior, this was likely a consequence of how the Bucket model handles soil moisture and its potential inability to keep up with evaporation rates during particularly dry times.

Monthly Precipitation (mm)

	2006								
	April			June			August		
	Mean	Bias	SD	Mean	Bias	SD	Mean	Bias	SD
PRISM	59.6	--	44.2	52.7	--	31.2	91.8	--	44.6
CLM4.0	70.6	+11.0	53.6	36.7	-16.0	26.2	77.3	-14.5	86.6
Noah-MP	64.6	+5.0	52.3	32.1	-20.6	22.8	98.0	+6.2	81.0
Bucket	85.1	+25.5	66.6	63.4	+10.7	43.4	75.7	-16.1	60.6
	2007								
	April			June			August		
	Mean	Bias	SD	Mean	Bias	SD	Mean	Bias	SD
PRISM	69.7	--	35.3	99.2	--	81.4	79.0	--	65.5
CLM4.0	94.5	+24.8	52.9	81.8	-17.4	55.9	35.7	-43.3	47.9
Noah-MP	84.4	+14.7	50.2	112.3	+13.1	110.7	46.1	-32.9	52.4
Bucket	98.4	+28.7	50.7	68.9	-30.3	59.6	27.7	-51.3	29.3
	2012								
	April			June			August		
	Mean	Bias	SD	Mean	Bias	SD	Mean	Bias	SD
PRISM	58.3	--	40.7	43.5	--	33.9	59.5	--	59.8
CLM4.0	62.7	+4.4	49.4	33.8	-9.7	34.5	61.1	+1.6	67.3
Noah-MP	54.4	-3.9	45.5	36.5	-7.0	40.8	66.4	+6.9	72.8
Bucket	88.0	+29.7	57.1	68.7	+25.2	52.5	38.7	-20.8	51.3

Table 3.4: Mean monthly precipitation, bias compared to PRISM, and standard deviation over the inner domain (4-km horizontal resolution) for the months of April, June, and August of 2006, 2007, and 2012.

The temperature bias was also computed for each land use type over the inner domain. Noah-MP performed the best overall with the lowest temperature bias (Table 3.5). Instances in which CLM4.0 had the smallest temperature bias either occurred in

land use categories not dominant to the SGP study region (i.e., wetlands and water bodies) or were not consistent across months. The Bucket model consistently showed a strong cool bias for each land use category. The magnitude of bias among the 3 LSMs increased as the warm season progressed (Table 3.5).

	April 2006			June 2006			August 2006		
	Bucket	Noah-MP	CLM4.0	Bucket	Noah-MP	CLM4.0	Bucket	Noah-MP	CLM4.0
Dryland Cropland/Pasture	-1.08	**0.15**	0.28	-0.26	**-0.01**	0.04	-9.40	**0.53**	0.70
Irrigated Cropland/Pasture	-3.04	**0.26**	0.47	-0.61	**-0.01**	0.10	-9.45	**0.53**	0.73
Mixed Dry/Irrigated Crops	-2.00	**0.25**	0.38	-1.01	**0.07**	0.22	-8.10	**0.79**	0.81
Mixed Cropland/Grassland	-1.63	**0.14**	0.25	-2.57	**0.44**	0.81	-7.48	**0.73**	0.76
Mixed Cropland/Woodland	-2.15	**0.21**	0.38	-3.30	**0.52**	0.86	-6.28	**0.73**	0.73
Grassland	-2.39	**0.13**	0.35	-5.12	**0.82**	1.19	-5.90	**0.72**	0.74
Shrubland	-2.52	**0.19**	0.42	-5.93	**0.86**	1.34	-5.60	**0.75**	0.86
Mixed Shrubland/Grassland	-2.66	**0.27**	0.43	-5.85	**0.89**	1.26	-5.25	**0.63**	0.81
Savanna	-2.52	**0.39**	0.47	-6.16	**0.94**	1.19	-4.26	**0.71**	0.82
Deciduous Forest	-2.53	**0.48**	0.54	-6.00	**0.83**	1.13	-4.47	**0.95**	1.06
Evergreen Forest	-2.55	**0.56**	0.57	-6.05	**0.89**	1.15	-4.75	**1.12**	1.16
Water Bodies	-2.64	0.67	**0.56**	-6.07	**0.84**	0.88	-4.73	1.20	**1.12**
Herbaceous Wetland	-2.59	0.88	**0.69**	-6.17	**0.83**	0.88	-4.71	1.26	**1.23**

Table 3.5: Mean temperature bias (°C) over the inner domain for each land use category common in the Great Plains region. April, June, and August 2006 are shown for the Bucket model, Noah-MP LSM, and CLM4.0 LSM. The value corresponding to the LSM with the lowest bias for each land use category is bolded for each month.

Point data from the ARM and AmeriFlux sites (Fig. 2.2) were also used for validation. Model output of temperature, SH, LH, and SWC were compared to site observations at Ozark, Missouri, and Mead, Nebraska (Fig. 3.14). While no LSM was clearly superior, similar patterns for associated temperature biases for each LSM evolved. Noah-MP and CLM4.0 failed to capture the patterns of peaks and troughs in SWC at the 10 cm soil level, and consistently underestimated the SWC magnitude. No clear conclusions emerged regarding which LSM performed best in simulating LH and SH fluxes in the comparisons at these 2 sites (Fig. 3.14).

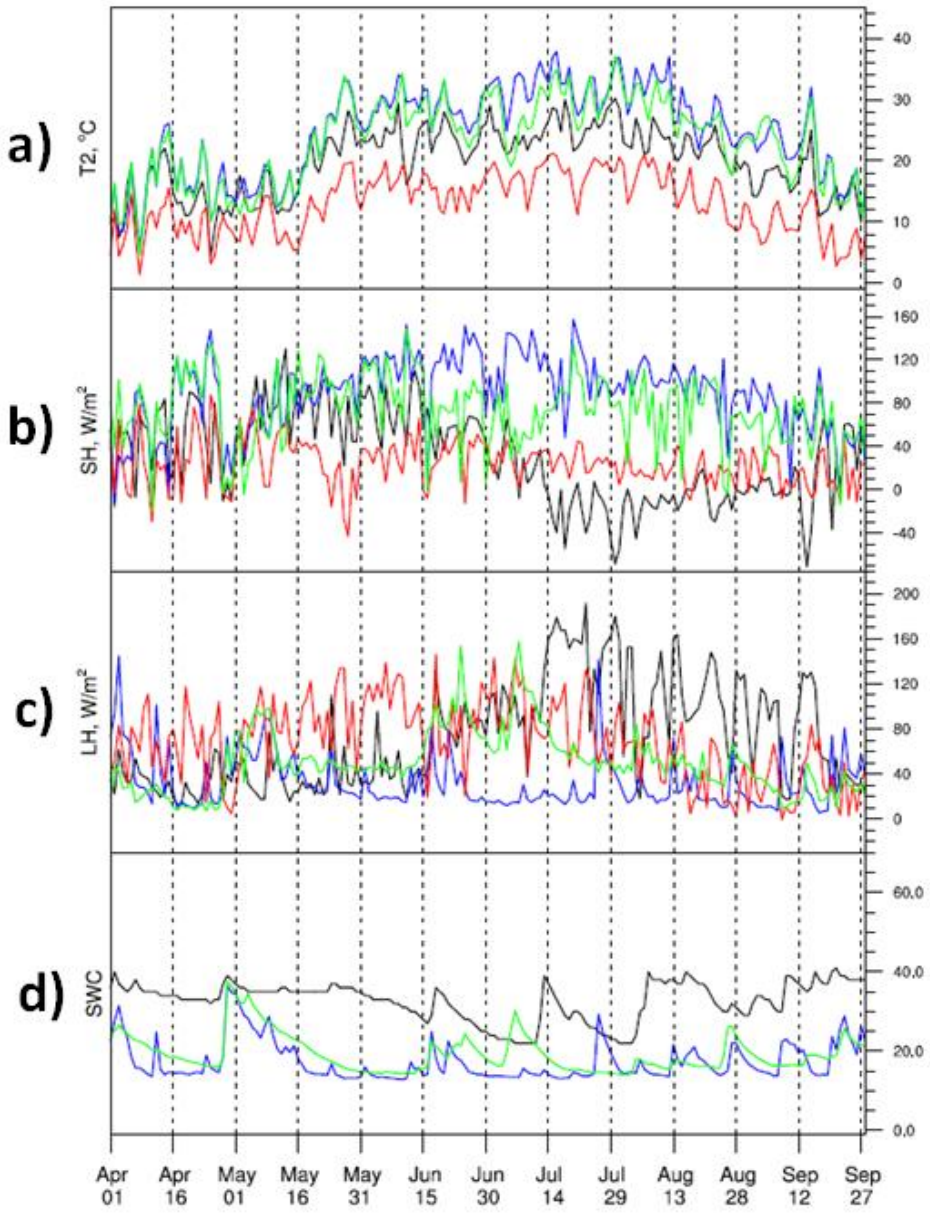

Figure 3.14: Observations (black line) and LSM output (CLM4.0 = blue line; Noah-MP = green line; Bucket model = red line) for the Mead, Nebraska, AmeriFlux site for the months of May-September for 2006. (a) is 2-m temperature, (b) is sensible heat, (c) is latent heat, and (d) is soil water content at 10 cm.

In an effort to diagnose potential reasons for these temperature and precipitation biases, the monthly mean ET and solar radiation received at the surface were calculated for the entire inner 4-km domain (Table 3.6). It was determined that the Bucket model in

general produced higher rates of ET compared to CLM4.0 and Noah-MP. The differences between the Bucket model and the two more sophisticated models were greatest during 2012, a drought year over the study year.

Evapotranspiration (mm)

	2006			2007			2012		
	April	June	August	April	June	August	April	June	August
CLM4.0	1.79	2.33	1.98	2.33	3.45	1.72	1.90	2.06	1.71
Noah-MP	1.45	2.42	2.14	1.94	3.54	2.04	1.64	2.36	1.82
Bucket	2.59	3.53	2.40	2.24	3.02	2.49	2.70	3.73	3.01

Solar Radiation Received At Surface ($W\ m^{-2}$)

	2006			2007			2012		
	April	June	August	April	June	August	April	June	August
CLM4.0	265.9	343.1	282.6	257.2	320.8	294.1	272.9	341.3	287.4
Noah-MP	266.7	342.3	278.9	255.4	321.7	290.7	276.6	342.8	283.1
Bucket	249.5	326.3	246.6	248.6	313.4	269.8	257.3	329.4	286.5

Table 3.6: Mean monthly evapotranspiration and solar radiation received at the surface over the inner domain (4-km horizontal resolution) for the months of April, June, and August of 2006, 2007, and 2012.

When comparing the monthly mean solar radiation received at the surface for each LSM, CLM4.0 and Noah-MP had higher values in general compared to those of the Bucket model (Table 3.6). To provide some idea of how these values compared to actual observations, AmeriFlux data from Mead, Nebraska was gathered and compared to the corresponding grid cells of each LSM (Table 3.7). In most months, the observed value of solar radiation at the surface was greater than that calculated by the Bucket model, but less than that of CLM4.0 and Noah-MP. In some instances, the observed value was lower than all 3 LSMs, with the Bucket model being the next lowest. This overestimate of solar radiation by WRF has been demonstrated in other studies such as Lu and Kueppers (2012) and Markovic et al. (2008).

Solar Radiation Received At Surface ($W\ m^{-2}$)
Mead, Nebraska AmeriFlux Site

	2006			2007			2012		
	April	June	August	April	June	August	April	June	August
AmeriFlux	202.1	289.3	221.63	230.02	266.7	134.9	233.2	282.5	259.3
CLM4.0	247.1	331.0	266.8	242.2	325.9	269.3	252.2	343.8	276.7
Noah-MP	242.5	327.9	245.1	240.4	320.7	264.2	261.1	334.9	273.7
Bucket	206.5	297.7	187.3	224.3	306.3	223.3	213.5	295.4	228.5

Table 3.7: Mean monthly solar radiation received at the surface at the Mead, Nebraska AmeriFlux site. AmeriFlux data represents actual observed data while LSM data is model computed for the appropriate grid point.

These results are consistent with what would be expected when examining them in a basic surface energy budget frame of reference, similar to that conducted in section I of this study. The Bucket model's inability to adapt to potentially rapidly changing soil moisture and evaporation rates, particularly in dry years, would lead to higher ET. Conversely, CLM4.0 and Noah-MP have better capabilities when it comes to calculating soil moisture and ET, but may not be able to fully grasp the extent of irrigation over the Southern Great Plains leading to lower ET. This would lead to more resultant environmental water vapor in the Bucket model than that of the two more sophisticated models. In addition to increased precipitation, one could infer more/less moisture would lead to more/less cloud cover which would lead to less/more downward solar radiation. A larger/smaller received solar radiation term in the surface energy budget will lead to a larger/smaller outgoing longwave radiation term and thus a higher/lower resultant temperature, assuming all else is equal. Of course this whole process of either over or under heating the ground could have a positive feedback on itself, thus further impacting the Bowen ratio and resultant ET and soil moisture.

This idea of each LSM either over or underestimating soil moisture and resultant ET was further explored by looking at the surface energy fluxes. The mean monthly

diurnal cycles of temperature, LH, and SH from the ARM and AmeriFlux sites were plotted for April, June, and August for the 3 study years (Fig. 3.15). All 3 LSMs generally replicate the diurnal cycle but differ in magnitude. Consistent with the results above, diurnal variation of 2-m air temperature in the CLM4.0 and Noah-MP simulations was greater than observed, while that from the Bucket model was less. The Bucket model tended to produce the largest peak in LH, which was, in general, an overestimate compared to observations (Fig. 3.15). Conversely, the Bucket model typically produced the lowest SH flux values for the diurnal cycle, in agreement with Bowen ratio arguments. As expected, the opposite was true for CLM4.0 and Noah-MP, overestimating SH and underestimating LH.

Again, examining these results in a surface energy frame of reference similar to section I, the resultant temperature biases can further be explained. As the Bucket model overestimates the partitioning to latent heating, more energy is going into a constant temperature process/phase change, or in this case, evaporation of soil moisture. By increasing the latent heating term, a higher vapor pressure would result, consistent with the idea of high ET discussed earlier. As less energy is used to heat the ground itself (SH), the outgoing longwave radiation term and thus the resultant temperature is less. A similar argument can be made for the over partitioning of SH by CLM4.0 and Noah-MP. As less energy is going into a constant temperature process such as evaporation, more energy is going into heating a comparatively drier ground surface and thus a higher resultant temperature.

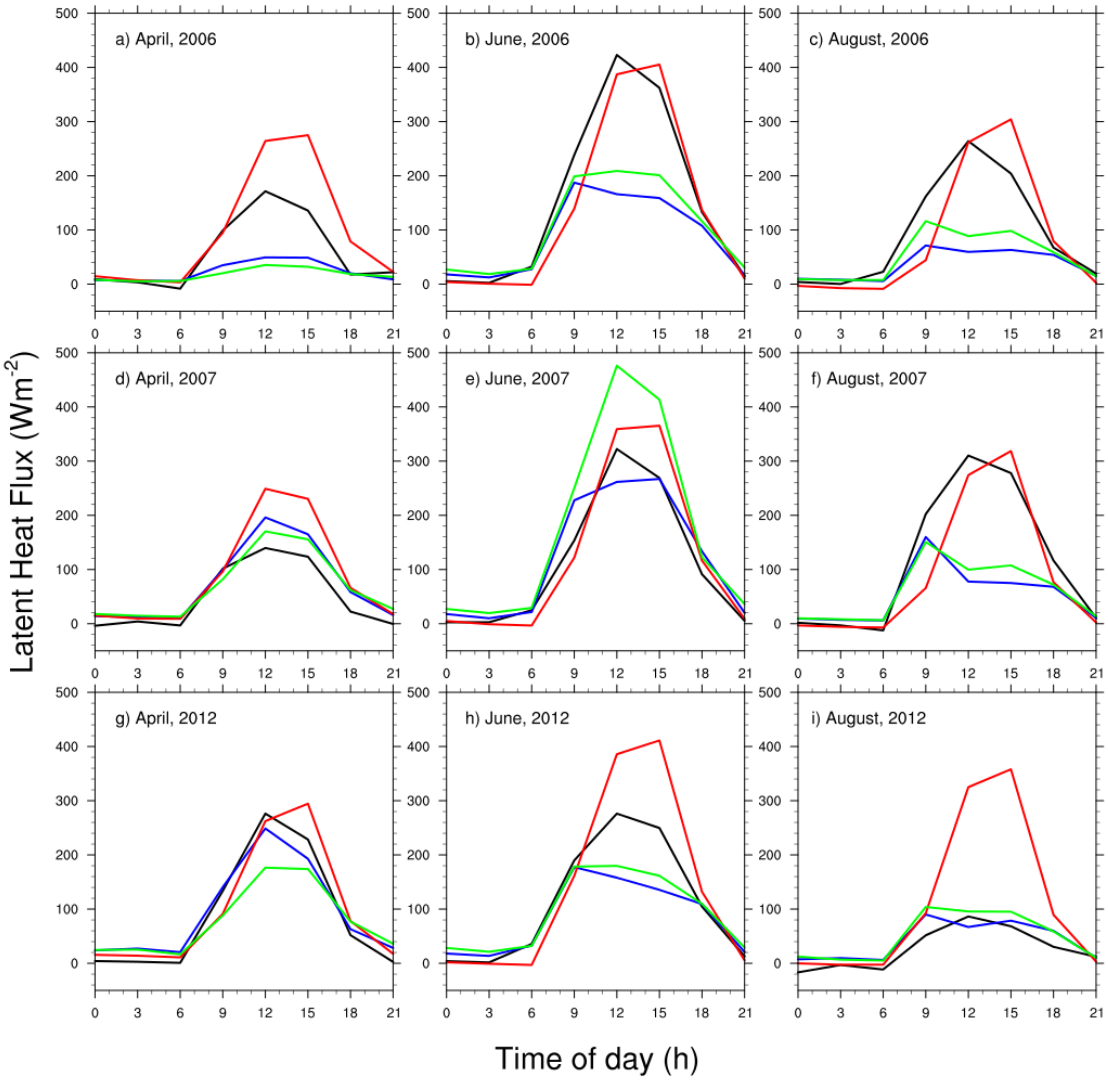

Figure 3.15: Diurnal cycle of latent heat flux at Ashton, Kansas, ARM site for the months of April, June, and August of 2006 (a-c), 2007 (d-f), and 2012 (g-i). Observed latent heat flux (black line), and output from CLM4.0 (blue line), Bucket model (red line) and Noah-MP (green line).

Chapter 4. Conclusions and Discussion

The relative capabilities of 3 LSMs coupled with WRF3.6 were examined in describing surface water and energy fluxes in the U.S. SGP for the warm seasons of 2006, 2007, and 2012. Model output was compared to PRISM data for mean monthly temperature and total monthly precipitation. Monthly mean ET and downward solar radiation were also computed for the study area. Additionally, model output for temperature, LH, SH, and SWC were compared to observations at four ARM and two AmeriFlux sites.

A warm bias in 2-m air temperature was found in CLM4.0 and Noah-MP, with an even larger cool bias in the Bucket model. These biases tended to increase as the warm season progressed. To diagnose reasons for these temperature biases, soil moisture, ET, downward solar radiation received and the surface energy partitioning between LH and SH were all examined. It was determined that both CLM4.0 and Noah-MP had a higher magnitude downward solar radiation compared to that of the Bucket model. The two more sophisticated models also showed lower values of ET and LH but higher values of SH compared to the Bucket model. A general underestimate of soil water content was also noted by CLM4.0 and Noah-MP compared to observations.

All of these results are consistent with a warm bias in CLM4.0 and Noah-MP and a cool bias in the Bucket model when examining them in a surface energy budget frame of reference. What is unclear is what the primary or original cause of the relevant biases was. For example, an underestimate of soil moisture in CLM4.0 and Noah-MP would lead to an underestimate of LH, and according to the Bowen ratio, an overestimate of SH. This would result in a lower magnitude of ET and the assumption that less environmental

water vapor could lead to less cloud cover and therefore an overestimate of downward solar radiation received at the surface. This would lead to a higher outgoing longwave radiation term and thus a warm 2-m temperature bias, as was observed in the two sophisticated models. On the contrary, one could make an argument that an original overestimate of downward solar radiation, which WRF has been shown to inherently have, could artificially dry out and heat the ground more quickly than what is observed in reality, thus leading to the underestimate of soil moisture scenario described above. The opposite scenario could be described for the Bucket model with an overestimate of soil moisture and its resultant surface energy fluxes as well as an underestimate of downward solar radiation and increased cloud cover.

Overall, the smaller temperature biases in CLM4.0 and Noah-MP are likely attributable to a better handling of soil moisture compared to the Bucket model. Both of the sophisticated models have more soil levels at which soil moisture is calculated and altered, as well as better capabilities handling hydrologic process in the rooting zone. This is in comparison to the restrictions the Bucket model faces with its soil moisture and ET calculations. This more accurate depiction of soil moisture is critical in the handling of energy partitioning between LH and SH. All 3 LSMs adequately simulated the diurnal variability of temperature, LH, and SH, but were shifted in magnitude suggesting their weaknesses lie in their overall handling of the processes that control these variables.

The simulation of precipitation was poorer with all LSMs than for temperature, as expected given the large temporal and spatial variability of precipitation events. All 3 LSMs produced similar patterns of wet and dry biases, again with the largest differences between CLM4.0/Noah-MP and the Bucket model. These differences between LSMs

were largest during the drought year of 2012, as were their biases compared to observations.

Of the two sophisticated LSMs included (CLM4.0 and Noah-MP), some differences existed but these effectively appeared to be random. No systematic bias or persistent pattern as to why one model performed better seemed evident and thus further in-depth analysis into these biases was not undertaken.

Variations in output from high-resolution regional models can be caused by many factors, such as large-scale remote forcing, model microphysics, cloud-precipitation physics, and convective parameterization schemes, all of which were held constant in these simulations. It is therefore clear that model output is sensitive to how each respective LSM handles, for example, soil moisture and vegetation canopy processes. CLM4.0 and Noah-MP are both more complex in allowing for sub-grid calculations and attempting to handle the relevant biophysics. As currently configured, however, they may not be able to adequately represent human influences such as irrigation, especially during drought years, or rapidly-changing land use in some areas, increasing error. Irrigation was shown to affect factors such as energy partitioning, VPD, and surface-air temperature difference. Future studies examining the effects of land use change and irrigation could help to close this gap between model simulations and observations.

It is important to consider the goals and resources of a study prior to choosing a LSM, as each has its advantages and disadvantages. For example, CLM4.0 is better equipped to handle differing vegetation types and thus may be best for studies directly examining this topic. This LSM also contains additional output variables, such as more expansive and deeper soil moisture and root info, which may be useful in some contexts,

as well as convective parameters pertaining to instability, precipitation type and cloud height/depth. However, CLM4.0 is also much more computationally intensive than Noah-MP, without necessarily providing better results in overall surface and atmospheric variables. Thus, it may not be feasible or necessary to use CLM4.0 if the effects of vegetation are not the primary topic of research. With this in mind, both CLM4.0 and Noah-MP seem to be scientifically viable options for examining the effects of land-atmosphere interactions on climate for the SGP region in the warm season, including the influences of historic land use change, while the limitations of the Bucket model with detailed surface energy calculations make it less suitable for such a detailed study.

REFERENCES

Bowen, I. S., 1926: The ratio of heat losses by conduction and by evaporation from any water surface. *Physical Review*, **27**, 779-787.

Budyko, M. I., 1961: *The Heat Balance of the Earth's Surface.* National Weather Service, U.S. Department of Commerce, Washington, D.C.

Carleton, A. M., J. Adegoke, J. Allard, D. L. Arnold, and D. J. Travis, 2001: Summer season land cover-convective cloud associations for the Midwest U.S. "Corn Belt". *Geophys.Res.Lett.,* **28**, 1679-1682.

Chang, J.-T., and P.J. Wetzel, 1991: Effects of spatial variations of soil moisture and vegetation on the evolution of a prestorm environment: A case study. *Mon. Wea. Rev*., **119**, 1368-1390.

Charney, J., P. H. Stone, and W. J. Quirk, 1975: Drought in the Sahara: A biogeophysical feedback mechanism. *Science*, **187**, 434-435.

Chen, F., C. Liu, J. Dudhia, and M. Chen, 2014: A sensitivity study of high-resolution regional climate simulations to three land surface models over the western United States. *J. Geophys. Res.: Atmos.,* **119**, - 2014JD021827.

Copeland, J. H., R. A. Pielke, and T. G. F. Kittel, 1996: Potential climatic impacts of vegetation change: A regional modeling study. *J. Geophys. Res.: Atmos.,* **101**, 7409-7418.

Daly, C., M. Halbleib, J. I. Smith, W. P. Gibson, M. K. Doggett, G. H. Taylor, J. Curtis, and P. P. Pasteris, 2008: Physiographically sensitive mapping of climatological temperature and precipitation across the conterminous United States. *Int. J. Climatol.,* **28**, 2031-2064.

Dudhia, J., 1989: Numerical study of convection observed during the Winter Monsoon Experiment using a mesoscale two–dimensional model. *J. Atmos. Sci*., **46**, 3077–3107.

Findell, K. L., E. Shevliakova, P. C. D. Milly, and R. J. Stouffer, 2007: Modeled impact of anthropogenic land cover change on climate. *J. Climate*, **20**, 3621-3634.

Hanson, K. -J., T. H. Vonder Haar, and V. E. Suomi, 1967: Reflection of sunlight to space and absorption by the earth and atmosphere over the united states during spring 1962. *Mon. Wea. Rev.*, **95**, 354-362.

Holt, T., D. Niyogi, F. Chen, M. A. LeMone, K. Manning, and A. L. Qureshi, 2006: Effect of land– atmosphere interactions on the IHOP 24–25 May 2002 convection case. *Mon. Wea. Rev*., **134**, 113–133.

Hong, S.-Y., J. Dudhia, and S.-H. Chen, 2004: A revised approach to ice microphysical processes for the bulk parameterization of clouds and precipitation. *Mon. Wea. Rev*., **132**, 103–120.

Hu, Q., S. Feng, 2012: AMO- and ENSO-driven summertime circulation and precipitation variations in North America. *J. Climate*, **25**, 6477-6495.

Huang, D. and Y Liu, 2015: A novel approach for introducing cloud spatial structure into cloud radiative transfer parameterizations. *Environ. Res. Lett*. **9**, 124022.

Jacobs, K., D. B. Adams, and P. Gleick, 2000: Potential consequences of climate variability and change for the water resources of the United States. U.S. National Assessment of the Potential Consequences of Climate Variability and Change, Cambridge University Press, 405–435.

Jin, J., N. L. Miller, and N. Schlegel, 2010: Sensitivity study of four land surface schemes in the WRF model. *Adv. Meteor.*, **2010**, 11.

Kain, J. S., and J. M. Fritsch, 1990: A one-dimensional entraining/detraining plume model and its application in convective parameterization. *J. Atmos. Sci.*, **47**, 2784-2802.

Kain, J. S., 2004: The Kain-Fritsch convective parameterization: An update. *J. Appl. Meteor.*, **43**, 170-181.

Koster, R. D., M. J. Suarez, 1995: Relative contributions of land and ocean processes to precipitation variability. *J. Geophys Res.: Atmos.,* **100**, 13775–13790**.**

Lawrence, D. M., K. W. Oleson, M. G. Flanner, P. E. Thornton, S. C. Swenson, P. J. Lawrence, X. Zeng, Z. Yang, S. Levis, K. Sakaguchi, G. B. Bonan, and A. G. Slater, 2011: Parameterization improvements and functional and structural advances in version 4 of the Community Land Model. *J. Adv. Model. Earth Syst.*, **3**, 27 pp.

Lu, Y., and L. M. Kueppers, 2012: Surface energy partitioning over four dominant vegetation types across the United States in a coupled regional climate model (Weather Research and Forecasting Model 3 Community Land Model 3.5). *J. Geophys. Res.: Atmos.,* **117**, - D06111.

Luo, Y. Q., and Coauthors, 2012: A framework for benchmarking land models. *Biogeosciences*, **9**, 3857-3874.

Lyons, T. J., H. Xinmei, P. Schwerdtfeger, J. M. Hacker, I. J. Foster, and R. C. G. Smith, 1993: Land–atmosphere interaction in a semiarid region: The bunny fence experiment. *Bull. Amer. Meteor. Soc.*, **74**, 1327–1334.

Mahmood, R., S. A. Foster, T. Keeling, K. G. Hubbard, C. Carlson, and R. Leeper, 2006: Impacts of irrigation on 20th century temperature in the northern Great Plains. *Global Planet. Change,* **54**, 1-18.

Mahmood, R., K. G. Hubbard, R. D. Leeper, and S. A. Foster, 2008: Increase in near-surface atmospheric moisture content due to land use changes: Evidence from the observed dewpoint temperature data. *Mon. Wea. Rev.*, **136**, 1554-1561.

Manabe, S. 1969. Climate and the ocean circulation – Part 1: The atmospheric circulation and the hydrology of the earth's surface. *Mon. Wea. Rev.*, **97**, 739-774.

Markovic, M., C. G. Jones, P. A. Vaillancourt, D. Paquin, K. Winger, and D. Paquin-Ricard, 2008: An evaluation of the surface radiation budget over North America for a suite of regional climate models against surface station observations, *Clim. Dyn.*, **31**, 779-794.

McPherson, R., D. Stensrud, and K. Crawford, 2004: The impact of Oklahoma's winter wheat belt on the mesoscale environment. *Mon. Wea. Rev.*, **132**, 405-421.

Mesinger, F., and Coauthors, 2006: North American regional reanalysis. *Bull. Amer. Meteor. Soc.*, **87**, 343-360.

Mlawer, E., J. Steven, J. Taubman, P. D. Brown, M. J. Iacono, and S. A. Clough, 1997: Radiative transfer for inhomogeneous atmospheres: RRTM, a validated correlated–k model for the longwave. *J. Geophys. Res.*, **102**, 16663–16682.

Mo, K. C., J. N. Paegle, and R. W. Higgins, 1997: Atmospheric processes associated with summer floods and droughts in the central United States. *J. Climate*, **10**, 3028 – 3046.

Mo, K., and J. Schemm, 2008: Droughts and persistent wet spells over the United States and Mexico. *J. Climate*, **21**, 980-994.

Nair, U. S., Y. Wu, J. Kala, T. J. Lyons, R. A. Pielke Sr., and J. M. Hacker, 2011: The role of land use change on the development and evolution of the west coast trough, convective clouds, and precipitation in southwest Australia. *J. Geophys. Res.: Atmos.*, **116**, *D07103.*

Niu, G., and Coauthors, 2011: The community Noah land surface model with multiparameterization options (Noah-MP): 1. Model description and evaluation with local-scale measurements. *J. Geophys. Res.: Atmos.*, **116**, - D12109.

Oglesby, R. J., and D. J. Erickson, 1989: Soil moisture and the persistence of North American drought. *J. Climate*, **2**, 1362-1380.

Oglesby, R. J., S. Marshall, J. O. Roads, and F. R. Robertson, 2001: Diagnosing warm season precipitation over the GCIP region from a GCM and reanalysis *J. Geophys. Res.: Atmos.,* **106**, 3357-3369.

Oglesby, R. J., S. Marshall, D. J. Erickson III, J. O. Roads, and F. R. Robertson, 2002: Thresholds in atmosphere-soil moisture interactions: Results from climate model studies. *J. Geophys. Res.*, **107**, 4224 – 4239.

Oleson, K. W., D. M. Lawrence, G. B. Bonan, M. G. Flanner, E. Kluzek, P. J. Lawrence, S. Levis, S. C. Swenson, and P. E. Thornton, 2010: Technical description of version 4.0 of the Community Land Model (CLM). NCAR, 266 pp. [Available online at http://www.cesm.ucar.edu/models/ccsm4.0/clm/CLM4_Tech_Note.pdf]

Paltridge, G. W., and Platt, C. M. R., 1976: *Radiative processes in meteorology and climatology*. Amsterdam ; New York: Elsevier Scientific Pub. Co..

Pielke, R. A., G. A. Dalu, J. S. Snook, T. J. Lee, and T. G. F. Kittel, 1991: Nonlinear influence of mesoscale land use on weather and climate. *J. Climate*, **4**, 1053-1069.

Pielke, R. A., 2001: Influence of the spatial distribution of vegetation and soils on the prediction of cumulus convective rainfall. *Rev. Geophys*., **39**, 151–177.

Pitman, A. J., 2003: The evolution of, and revolution in, land surface schemes designed for climate models. *Int. J. Climatol.,* **23**, 479-510.

PRISM Climate Group, Oregon State University, http://prism.oregonstate.edu, accessed 17 Feb 2015.

Schubert, S. D., M. J. Suarez, P. J. Pegion, R. D. Koster, and J. T. Bacmeister, 2004: Causes of long-term drought in the U.S. Great Plains. *J. Climate*, **17**, 485-503.

Skamarock, W., J. Klemp, J. Dudhia, D. Gill, D. Barker, W. Wang, and J. Powers, 2008: A description of the Advanced Research WRF version 3. NCAR Tech. Note NCAR/TN-4751STR, 113 pp.

Stern, M. E., and J. S. Malkus, 1953: The flow of a stable atmosphere over a heated island, Part II. *J. Meteor.*, **10**, 105-120.

Steyaert, L. T., R. G. Knox, 2008: Reconstructed historical land cover and biophysical parameters for studies of land-atmosphere interactions within the eastern United States. *J. Geophys. Res.: Atmos.,* **113**: D02101.

Subin, Z. M., W. J. Riley, J. Jin, D. S. Christianson, M. S. Torn, and L. M. Kueppers, 2011: Ecosystem feedbacks to climate change in California: Development, testing, and analysis using a coupled regional atmosphere and land-surface model (WRF3-CLM3.5). *Earth Interactions*, **15**, 1-38.

Taylor, C. M., E. F. Lambin, N. Stephenne, R. J. Harding, and R. L. H. Essery, 2002: The influence of land use change on climate in the Sahel. *J. Climate*, **15**, 3615-3629.

Trenberth, K. E., A. Dai, R. M. Rasmussen, and D. B. Parsons, 2003: The changing character of precipitation. *Bull. Amer. Meteor. Soc.*, **84**, 1205-1217.

Weaver, C. P., 2004: Coupling between large-scale atmospheric processes and mesoscale land–atmosphere interactions in the U.S. Southern Great Plains during summer. Part II: Mean impacts of the mesoscale. *J. Hydrometeor.*, **5**, 1247–1258.

Wei, J., P. A. Dirmeyer, Z. Guo, L. Zhang, and V. Misra, 2010: How much do different land models matter for climate simulation? Part I: Climatology and variability. *J. Climate*, **23**, 3120–3134.

Wilhite, D. A., 2000: Drought as a natural hazard: concepts and definitions. Droughts: A global assessment, D.A. Wilhite, Ed., Routledge, 3-18.